Review Article

Fahmi Imanullah, Eko Surojo* and Aditya Rio Prabowo

# Development and current milestone of train braking system based on failure phenomenon and accident case

https://doi.org/10.1515/jmbm-2025-0053
received September 04, 2024; accepted March 04, 2025

**Abstract:** Efficient and safe transportation needs are coveted by every human being. One mode of transportation that has many enthusiasts, especially in the land sector, is the train. The development of trains from time to time has a final destination to create a safe and comfortable mode of transportation from failure and accidents. This article discusses the development of braking systems, braking system failures, financial losses that occur, the use of advanced materials in braking systems, and the manufacturing process. This article is expected to be a reference in supporting the realization of rail as a public transportation on land with a low accident and failure level.

**Keywords:** train braking system, safety, advanced materials

## 1 Introduction

The development of transportation modes continues to grow over time. Humans initially walked on foot and then began using animals as a means of transportation. Until now, many types of transportation modes have sprung up both land, sea, and air. Each mode of transportation was created to facilitate human activities. One of the most popular modes of mass transportation, especially on land, is the train [1–3]. The trains are more in demand because of comfort, safety, cost, and time accuracy factors [1,4].

Research related to trains is continuously developed to support human activities, starting from the development of the railroad power system, railroad navigation systems, wagon systems, railroad braking systems, and so forth [5–8]. In general, each system must go through checking to match the existing functions and standards. The material to be used needs to be examined about its mechanical characteristics, to get superior traits such as fatigue and wear resistance, hardness and strength, and also resistance to corrosion [9,10]. All fields of research have one goal, namely, to improve the efficiency of the railroad industry as well as to support the safety of the trip [4,11].

In general, train accidents in the world still often occur ranging from slipping cars, navigation system errors that cause accidents, collapsed rail conditions, damaged braking system conditions, and so forth [12,13]. For this reason, this article will discuss the development of a braking system based on failure phenomena and accident cases to be used as further consideration.

## 2 The development of technology in a macro braking/railroad system

The development of the braking system on the train was slow for about 100 years from 1853, when Morse submitted a patent depicting a cast iron brake block [14]. The need for safety continues to increase with the development of the times. This is possible to continue to develop a safe braking system for trains. Fast trains such as Train à Grande Vitesse in France and Japanese Shinkansen introduce a new friction braking model consisting of metal bearings that are interred and steel discs, which we often call braking discs/disk brakes.

Research conducted by Dolbear and Watson suggested to maximize the lifetime of brake pad and rotors/discs and also explained that heat on discs needs to be distributed evenly [14]. This needs to be done to avoid not only the formation of hot spots that cause the brake pad to wear out faster but also cracks on the discs due to thermal stress. To

* **Corresponding author: Eko Surojo**, Department of Mechanical Engineering, Universitas Sebelas Maret, Surakarta, 57126, Indonesia, e-mail: esurojo@ft.uns.ac.id
**Fahmi Imanullah, Aditya Rio Prabowo:** Department of Mechanical Engineering, Universitas Sebelas Maret, Surakarta, 57126, Indonesia

fulfill this, the brake pad must be able to adjust to the contour of the disc.

In 1988, Roe explained about the train in New Zealand. In the braking system, locomotive section uses the full analog pneumatic Davies and Metcalfe P85 [15]. Each cabin is equipped with an automatic train brake and independent locomotive brake controller that is pneumatic associated with an automatic brake control unit and locomotive installed in brake equipment frames. Automatic brakes can be graduable in the application, but selector on the controller give the release option that can be graduable or directly. Independent brakes can be graduable in applications and releases and have a pilot valve operated by buttons to allow automatic brake release in the locomotive. The driver and assistant each have an emergency valve "panic button" that ventilated brake pipe directly into the atmosphere. Electronic Equipment Standard New Zealand railroad is installed. This is rearranged by operating the vigilance pedal or by moving the power handle, the electric brake handle, or sounding the horn. Regenerative electric brakes function as speed-retaining brakes on downhill tracks. This is operated by a separate controller positioned next to the power handle and can only be operated when the power grip is in an off position. Electric brakes and independent brakes can be operated simultaneously if needed, but the electro-pneumatic interlock valve holds automatic brakes in the locomotive until the dynamic braking efforts fade [15].

**Table 1:** Speed *vs* friction characteristic [16]

| Train speed (km/h) | Horsepower generated per wheel | Brake shoe friction (μ) |
|---|---|---|
| 30 | 21.08 | 0.146 |
| 40 | 33.30 | 0.172 |
| 50 | 45.90 | 0.204 |
| 60 | 64.40 | 0.223 |

Mercer explained the parameters in the braking process that refers to the standards made by the American Association of Railways as follows [16]:

1. Train control must be such that the train can be slowed or stopped anywhere on the gradient within the signal distance.
2. Amount of brake required to balance grade. This implies that the number of brakes needed to balance the value must be less than the maximum available, so that adequate margins of retarding force and horsepower are always available to slow down or stop trains.

Table 1 shows the speed *vs* friction characteristic data used. The brake block specifications used in this study are shown in Table 2.

In the world of transportation, the discovery of the wheels is the most important discovery. The use of wheels allows transportation that initially shifted with high frictional levels turn into shifting with a lower friction level. The use of wheels in the world of railroad Apian was found in the fifteenth century in coal mines in Germany, which was used on wood rails. The whole metal wheel was discovered in 1775 by Antonien Hutte (Figure 1). Figure 1 is drawn based on information and reference [17]. This wheel is made completely from cast iron, which has a weakness of wear resistance.

The cast iron construction wheel was further developed in 1827 into a composite design that utilized a wooden core with a wrought iron outer layer. This principle of combining different materials was later widely adopted in Europe, as evidenced by an illustration from a German source dated 1849. In 1849, Germain Morel in France patented the process of making a continuous wrought iron ring for the railroad tires. Once again, the poor resistance of this product makes it unsatisfactory economically, but in 1865, Cammell from the works of Shefield and Crewe in London North Western Railway produces Bestsemer steel roll tires. This provides a long-term solution to problems and initiating the process that continues to this day.

**Table 2:** Brake block formulation type X627 [16]

| Physical properties | Test parameters | | Unit | Test values | |
|---|---|---|---|---|---|
| Density | | 20°C | g/cm$^3$ | | 2.12 |
| Tensile strength | 20°C | 250°C | daN/cm$^2$ | 101.3 | 70.8 |
| Compressive strength | 20°C | 250°C | daN/cm$^2$ | 838 | 660 |
| Shear strength | | 20°C | daN/cm$^2$ | | 108 |
| Hardness | | | Rockwell 'R' | | 90 |
| Modulus of elasticity in compression | | 20°C | daN/cm$^2$ | | 9,650 |
| Specific heat | | | Cal/g | | 0.23 |
| Thermal conductivity | | | J/m/s/°C | | 0.8 |

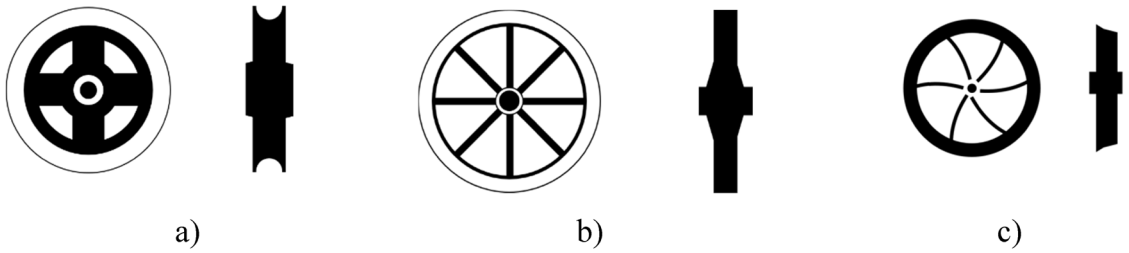


**Figure 1:** Wheels made of cast iron 1775 from Antonien Hutte (a) No. 144, (b) No. 145, and (c) No. 146 [17].

Overall, the period between war and immediately after World War II was one of the stabilities in the manufacture and use of wheels, especially in Europe. In North America, although the situation in connection with the locomotive wheels and training is equally stable, the problem of growing for the wheels of cast iron carriages is wear [17].

In 1986, Berndt and Schweiger also explained about the railroad braking system in the form of a disc consisting of two brake lining and one rotor [18]. Wilkinson divides braking in general into two types, mechanical and electric braking. Mechanical braking includes braking brakes with tread braking and disc braking. However, electric braking is of the rheostatic and regenerative [19].

Hasegawa and Uchida explained several classifications in the braking process based on the mechanism as shown in Figure 2. Figure 2 is drawn based on information and reference [20].

According to Fletcher, the basic feature of all regenerative braking schemes is that traction motors are effectively used as generators, converting mechanics into electrical energy [8]. This form of electric braking, or "dynamic" has been widely used, especially in electrical locomotives. Historically, the electrical energy obtained in braking has been scattered in the locomotive in a resistor or rheostat. This type of braking is referred to as a rheostatic braking.

Benseddiq *et al.* explained about the shape of the railroad brake lining based on UIC (Union Internationale des Chemins de Fer) [21]. This brake lining consists of two parts. The first part as a friction material (composite material consisting of an organic matrix and short fiber reinforcement, for example, steel, iron). The second layer is a flexible subtract. In the middle, there is one horizontal groove and two vertical grooves.

Desplanques *et al.* explained the testing method using the type of pin on disk that is used to facilitate the limitations of laboratory scale research but still able to represent the real conditions [22]. According to Desplanques, the brake block testing method is divided into two methods of braking, "stop braking" and "drag braking" [22]. Stop braking testing is done by turning the disk according to the desired speed and then disconnecting the current received by the electric motor. Flywheel stores inertia energy so that it keeps the disk spinning. Then the brake pad is emphasized until the disk stops. Drag braking testing is done by turning the disk according to the desired speed and then conducted pressing the brake lining for a certain time.

According to the Hecht Modern brake lining material is a type of composite. This material demonstrates constant frictional behavior with respect to velocity, as well as a coefficient of friction that is notably higher than cast

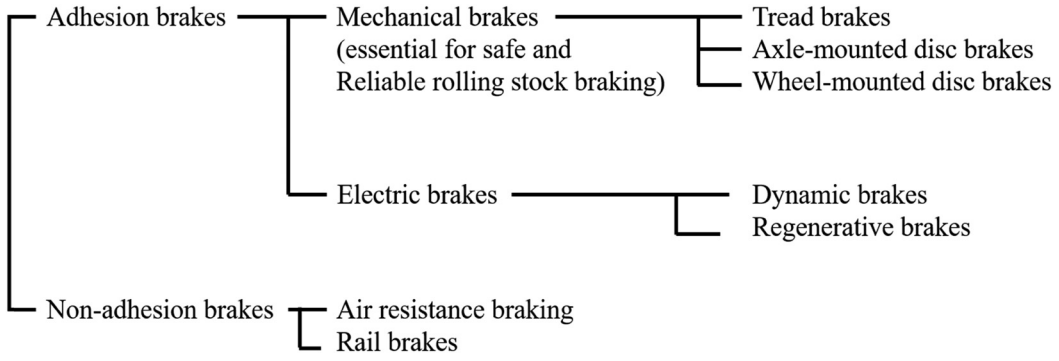


**Figure 2:** Braking mechanisms [20].

iron, up to μ of 0.4 [23]. The higher friction coefficient of the brake block reduces the braking force required. However, the issue of high thermal loading on the wheel surface during operation at high speeds is of critical importance. The friction characteristics remain relatively constant, and the braking force is directly proportional to the speed. This is in contrast to the braking force characteristics of cast iron brake blocks, which demonstrate a decrease in force over time. Therefore, in order to ensure that the braking force remains within the prescribed limits, it is essential to employ a method comparable to that of cast iron brake blocks. Further advantages of composite and sintered materials are the rate of wear, which is much lower than cast iron. Composite brake blocks have a wear resistance five times longer than cast iron brake blocks. This not only compensates for higher costs per brake block but also provides high value returns by reducing the need for maintenance downtime, space for large workshops and labor.

According to Grosse, the disc brakes are applied to modern high-speed trains. Unlike the train brake block, the disc brake is not heated during braking. The absence of this annealing effect can result in the smoothing of the wheel sector and the formation of cracks under the site. Residual pressure formed during service plays an important role in the initiation of cracks and the process of cracking. Neutron diffraction is used to investigate the structural reasons for the measurement of damage strain in the wheel area [24].

Nankyo explained that the performance of the train vehicle brake was represented by an index called "deceleration," which was a negative acceleration [25]. Vehicles equipped with electricity-controlled pneumatic brake systems are designed to apply the braking power assigned to the brake handle notch in accordance with the planned deceleration. Pneumatic systems are an important part of the deceleration process.

Cartigny explained the breakthrough about the cooled brake lining using liquid. The new type of brakes recommended in this article are original because the brake function is reversed compared to the actual use; the brake pad is metallic and absorbs the friction heat generation, while the disk supports friction and is thermal barrier [26]. Refrigerant fluid flows in the channel drilled in the brake pad. The cooler is carried by the primary channel called the collector to the secondary channel. Wall heat exchange allows the evacuation of friction heat absorbed by the brake pad. The purpose of cooling the brake pad is to transmit to the brake pad the maximum amount of friction heat produced to weaken the energy stored in the disc between two braking.

Handoko explained that most of the good's trains are equipped with a braking system that uses compressed air (pneumatic brakes) to produce the necessary strengths and apply them to the wheels through bearings or discs. The typical air brake system used in goods carriages in North America and Australia flows compressed air along the train through a pipe with a valve that controls the level of pressure to produce the necessary braking power [27].

Vernersson explained the four general block configurations used in the tread braking system [28]. In Europe, the block setting has a standard name. The length of the individual brake block is usually 320 mm when one block per block holder block is used and 250 mm when two blocks per holder are used (tandem configuration). The heat partition between blocks and wheels is influenced by block configurations because this affects the total contact area, total heat capacity, and also cooling conditions.

Douglas explained that regenerative braking is a technology that allows the recovery of vehicle braking energy as electricity [29]. The system works by utilizing the ability of an electric motor to act as a generator. In some cases, it is possible to recover more than one-third of the total traction energy using this method, significantly reducing network energy costs. Captured braking energy is typically used directly by vehicles to power heating, ventilation, air conditioning, and lighting. Literature recent reviews show that the steps of the main regenerative energy saving are: Optimizing the operating schedule to maximize the exchange of energy between vehicles, applying substations that can be reversed to supply regenerated energy to the national electricity network, and using a roadside storage system or in on the ship to capture and reuse braking energy when needed [29]. Some studies also focus on ensuring effective regeneration to maximize energy recovery by modifying a vehicle braking system or track.

Samec explained the disc brake, calculated as a safety component. Therefore, its reliability as long as the service is very important. Disc brakes are exposed to large thermal pressure during braking. In addition to substantial mechanical strength, the friction heat generation is very high. In the heavy task brake application, the heat flux in the interface is the order of $MW/M^2$ [30]. The heat produced during braking causes an increase in temperature in the interface, which spreads quickly through the brake components. Such a severe thermal process modifies the friction of the material in contact, causing wear and, on a large scale, produces component deflection. All of these changes must affect brake performance and life. A number of certain train disc brakes, made of gray iron, showed a crack only after a few thousand kilometers.

Vakkalagadda explains the regulatory scheme used to get the friction characteristics of the brake block. Number of brake blocks and brake loads per brake block used to match the typical field conditions Table 4. Different brake block dimensions used in the experiment are shown in Table 3. As seen from the experimental regulation scheme,

the flywheel is added to the shaft (where the wheels are installed) to ensure that the kinetic energy of rotation in accordance with the trendline velocity given matches the kinetic energy per wheel at the rail speed given and the burden of the axle. Direct current motor (DC) is used to reach the angle velocity specified for the wheels. After the desired speed is reached, the motor is released and the brake is applied. Brake load is used (Table 4) according to the typical brake load applied in pressure.

Sawczuk examined the effect of vibrations formed on a disc braking system which is given a sensor to find out the vibrations that occur [32]. Soma explained during the braking operation, the brake block was pressed to the surface of the revolving wheel and the kinetic energy and the train potential energy were converted into heat, which was produced in the brake block and wheel interface [33]. The friction heat produced during braking is distributed, with different proportions, between brake block and wheels.

Research conducted by Lu *et al.* uses tools that describe the performance of the brake lining. The main component consists of the drive module, flywheel, control module, emphasis module, and friction test components [34]. The test scheme can be seen in Figure 3. Figure 3 is drawn based on information and the study by Lu *et al.* [34]. Table 5 illustrates milestone development of technology in a macro braking/railroad system.

## 3 Failure, accident, and technical loss from the braking/railroad system

Material fatigue in the contact area of railway wheels is a crucial failure mechanism. Although the wear of this layer of surface in general is not a threat to direct safety, it affects the cost and competitive power of rail transportation. The increasing operational speeds and axle loads in contemporary railway systems have prompted a pressing need to enhance our understanding of wheel surface fatigue.

**Table 3:** Dimensions of brake blocks used in experiments [31]

| Brake block type | Dimensions (mm) | | | |
|---|---|---|---|---|
| | Radius | Width | Thickness | Length |
| K and L-type used in locomotive | 550 | 85 | 55 | 360 |
| K-type used in wagons | 505 | 85 | 58 | 300 |
| L-type used in wagons | 425 | 80 | 58 | 38 |

**Table 4:** Parameters used in full scale stop braking experience [31]

| Brake block type | Brake load per brake block (kN) | Number of brake blocks per wheel | Wheel diameter (mm) | Load per axle (tons) | Speed (km/h) |
|---|---|---|---|---|---|
| Cast iron | 25, 30, and 35 | 2 | 915 | 16.25 | 50–140 |
| K-type used in locomotives | 35 and 49 | 1 | 1,092 | 21 | 40–160 |
| K-type used in wagons | 11, 22, and 33 | 1 | 1,000 | 25 | 30–120 |
| L-type used in locomotives | 35 | 2 | 1,092 | 18.8 | 40–120 |
| L-type used in wagons | 24, 44 | 1 | 840 | 22.9 | 40–120 |

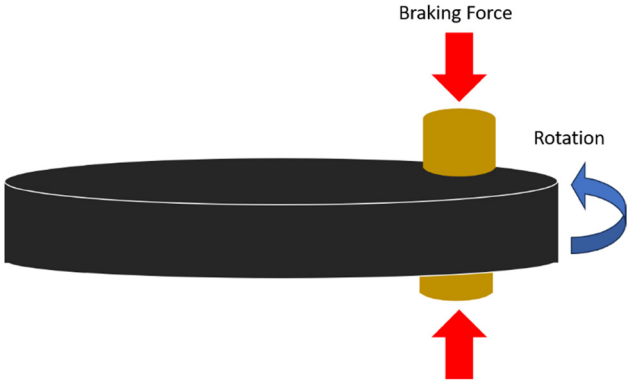


**Figure 3:** Schematic test [34].

Spalling and shelling of these two names are given by French people or often called skin peeling, or breakdown of footprint surface materials. Pieces of a depth of 25 mm × 2 mm disappeared from the rolling path [17].

The first cause is basically the loss of wheel and rail adhesion during braking, known as slide wheels. Extreme cases are characterized by an average tread because the wheel lock is complete at low speed, but loss of adhesion at a higher speed carries smaller shooting patches, which can ultimately extend throughout the tread. Slips between wheels and rails produce a local heater and rapid cooling that produces a martensite layer to a larger depth (2 mm) than a thin martensite area due to tread braking. In the context of wheel operational conditions, it is hypothesized that contact stresses acting beneath the tread surface initiate cracks at the boundary between the martensite and the heat-unaffected zone.

According to Kumagai *et al.*, there are several defects on the railroad wheels including [35]:

- Flat

Flats are classified into three modes - single flat, spot flat, and continuous flats. A single flat is an oval-shaped damage area caused by the locking axis in a running car and is often observed with an axle trailer. A spot flat is a small single set. A continuous flat, long and slim, caused when the wheel slipped on the rail without a wheel lock. This flat is likely to occur with a motorcycle car wheel in particular. Plastic flow when the material is often observed.

- Shelling

The shelling generally comes from thermal cracks aimed. At the surface area of the martensite tempered, thermal cracks are connected together. As a result, the shelling of fragments can occur with a hollow hole about 1 mm. This type of crack developed easily in the wheels as a result of the presence of water or snow. Fatigue from the tread grows in the area and eventually increases the results of the shelling. The shell pattern is observed on the face of the scale shell. Thin skin shelling, which is very thin and shallow, is produced along the circumference where with a width of about 10 mm.

- Thermal cracks

Tensile stress on the wheel tread is produced by a large braking force in a circular direction. In this condition, a straight-line crack is produced parallel to the direction of the wheel. This crack is called hair cracks. Hairline cracks are likely to be produced when the remaining tensile stress causes isotropy on the hot-spot surface. The lateral friction force on the wheel tread, because it slipped into the curve, produces a tensile stress in various directions. Under this condition, cracks in the arbitrary direction appear at time.

According to Day *et al.*, cracks can also occur in general in the radial direction in the disc or in the axial direction in the case of drum-brakes. This definite crack propagation shows a high stress. A combination of high temperatures and high pressure can cause plastic flow on the surface, and this will induce the tensile on the surface when the latter becomes cold. If a high work rate produces high compressive plastic strain, the high gradient is developed on the friction surface and high tensile stress in cooling, which may be enough to cause surface failure in one brake application. Cracks in the end can be so big that disc or drum failure occurs [36].

According to Kalousek *et al.*, there are several types of defects on the railroad wheels including wheel shelling, wheal thread wear, and brake shoe metal pick up [37].

Meizoso examined the estimated cracks on the railroad wheels through a computer program for the prediction of the life of the railroad wheel's life to combine elastoplastic calculations of the residual stress caused by braking shoes and revolving contact pressure alternately. The possibility of unstable surface crack propagation, cracked capture, fatigue propagation through stress, and cracking detention when reaching the threshold value has been calculated. The estimated method for the prediction of crack growth is used to provide a limit for the front position of instant cracks and estimated cracks in a short computing time [38].

According to zerbst, the growth of fatigue cracks in the wheels can cause loss of the wheel (spalling) or to the radial crack extension with the consequences of the release of press installation between the wheels and rails. The results can be damaged rails and vehicle components or even slip. In connection with the initiation of fatigue cracks, it must be distinguished between the wheels of wet vehicles and the wheels of dry vehicles [39].

**Table 5:** Milestone development of technology in a macro braking/railroad system

| Milestone | Author | Title | Important remarks | Ref. |
|---|---|---|---|---|
| 1985 | D. T. Wilkinson | Electric Braking Performance of Multiple-Unit Trains | The relationship between mechanical braking and electrical braking from time to time | [19] |
| 1986 | P. J. Berndt and W. Schweiger | Experimental and Theoretical Investigation of Brake Squeal with Disc Brakes Installed in Rail Vehicles | Clarification of the causes of brake squeals that propagate through structure and air | [18] |
| 1987 | C. I. Mercer | Medium Friction Non-Metallic Composition Brake Shoes as Direct Replacement for Cast Iron Brake Shoes on Rolling Stock | Better braking has been obtained by this middle class brake lining compared to cast iron brake lining | [16] |
| 1987 | S. Wise | Railway Wheelsets-A Critical Review | A brief history of the evolution of wheelsets and then outlines the changes that have occurred in their design in the last 30 years, mainly due to changes in diesel and electrical traction | [17] |
| 1988 | M. J. Roe | Electric Bo-Bo-Bo Locomotives for New Zealand Railways | Provision of regenerative brakes offers significant energy savings | [15] |
| 1991 | R. G. Fletcher | Regenerative Equipment for Railway Rolling Stock | Braking regenerative system in both DC and AC systems | [8] |
| 1994 | K. D. Dolbear and J. C. Watson | The Development of Friction Pairs for Intermediate to Very High Duty Railway Applications | Potential use of disc brakes and ceramic materials for the future | [14] |
| 1996 | N. Benseddiq, D. Weichert, J. Seidermann, and M. Minet | Optimization of Design of Railway Disc Brake Pads | The structure of the brake pad layer consists of the first layer is the friction material, the second layer is the elastic substrate, and the third layer is the rigid back plate | [21] |
| 1999 | Izumi Hasegawa and Seigo Uchida | Braking Systems | All vehicles have several braking devices | [20] |
| 2001 | Y. Desplanques, G. Degallaix, R. Copin, and Y. Berthier | A Tribometer for the Study of Materials Under Railway Braking Conditions | Their comparison with test results achieved on a full scale bench makes it possible to conclude their excellent representation | [22] |
| 2001 | M. Hecht | European Freight Vehicle Running Gear: Today's Position and Future Demands | Reduction of inspection time and brake checking time, lower weight, lower noise emissions, and lower lateral path force | [23] |
| 2002 | M. Grosse, M. Ceretti, and P. Ottlinger | Distribution of Radial Strain in a Disc-Braked Railway Wheel Measured by Neutron Diffraction | Differences in the distribution of radial strain between sectors containing cracks and sectors that are not damaged | [24] |
| 2003 | M. Nankyo, T. Ishihara, and H. Inooka | Feedback Control of Brake System on Railway Vehicle Considering Non-Linear Property and Dead Time | The controller design for the control tracking control and the system compensates for the dead time is proposed | [25] |
| 2004 | F. Cartigny, P. Dufrénoy, and B. Desmet | A thermal analysis of a new railway brake concept using liquid cooling | The concept of liquid disc brakes is very dependent on the control of heat flux propagation time due to friction from the interface to the cooling tract | [26] |
| 2006 | Y. Handoko and M. Dhanasekar | An Inertial Reference Frame Method for the Simulation of the Effect of Longitudinal Force to the Dynamics of Railway Wheelsets | The numerical model of one wheelset contained in a bogie frame that experiences longitudinal power with varying severity | [27] |
| 2007 | T. Vernersson | Temperatures at railway tread braking. Part 1: Modelling | The numerical model is used to investigate the temperature of blocks and wheels during the braking process | [28] |
| 2011 | B. Šamec, I. Potrč, and M. Šraml | Low cycle fatigue of nodular cast iron used for railway brake discs | Young's modulus of cast iron is relatively stable, while the tensile strength decreases as the temperature increases | [30] |
| 2015 | H. Douglas, C. Roberts, S. Hillmansen, and F. Schmid | An assessment of available measures to reduce traction energy use in railway networksHeather | Comparison of energy savings that can be achieved from various steps depending on the type of route, urban, between cities, and high speed | [29] |
| 2015 | M. R. K. Vakkalagadda, D. K. Srivastava, A. Mishra, and V. Racherla | Performance analyses of brake blocks used by Indian Railways | The type of brake block used in India is generally divided from cast iron and composite | [31] |

(*Continued*)

**Table 5:** *Continued*

| Milestone | Author | Title | Important remarks | Ref. |
|---|---|---|---|---|
| 2021 | W. Sawczuk, D. Ulbrich, J. Kowalczyk, and A. Merkisz-Guranowska | Evaluation of wear of disc brake friction linings and the variability of the friction coefficient on the basis of vibroacoustic signals | The vibrational signal produced by the friction layer provides information on its wear and offers an evaluation of the braking process, that is, changes in the average friction coefficient | [32] |
| 2021 | A. Somà, M. Aimar, and N. Zampieri | Simulation of the thermal behavior of cast iron brake block during braking maneuvers | Modeling finite element method is able to predict contact temperatures between wheels and brake lining | [33] |
| 2022 | C. Lu, X. Jiang, X. Chen, and J. Mo | Experimental study on the evolution of friction and wear behaviours of railway friction block during temperature rise under extreme braking conditions | The phenomenon of friction and wear in the brake block will change significantly and are interrelated with each other along with changes in temperature | [34] |

- The initiation of surface cracks in vehicle wheels with brake blocks is attributed to cyclic thermal loads that occur during braking. The braked wheel tread undergoes periodic heating due to friction with the brake blocks and cooling by the rails. It is imperative to acknowledge that the heating occurs unevenly along the circumference of the wheel, concentrating in areas designated as "hot spots," where temperatures can reach 540°C. Temperatures in excess of 840°C have also been documented. Subsequent contact with the rails precipitates rapid cooling due to high heat transfer. This uneven cooling process leads to substantial thermal stresses within the wheel rim.
- Initiation of surface cracks and subsurfaces on the wheels of the vehicle-disk. In the contact zone, stress deformation develops combined with residual stress generations and some strain hardening. At a high load level there is no elastic shaking. Conversely, each new load cycle increases plasticity and finally the accumulation of deformation exceeds the ductility of the material, this phenomenon is called ratcheting.

According to Dufrenoy *et al.*, the surface analysis of the damaged brake disc friction in the service was first done to identify two types of cracks. Stressfully with this analysis, numerical simulations are carried out to determine the thermomechanical loading due to successive braking, providing additional indications about the mechanism of damage. The results show that thermal fatigue occurs with the superposition of the friction effect. Surface analysis of damage and numerical calculations provides valuable information about the mechanism of failure and will lead to an increase in disc brake design to improve their performance.

The train brake disk experiences severe thermomechanical loading, which can provide cracks on the friction surface, which leads to their initial replacement. Observation of damage from several out-of-order discs was carried out, showing the thermal fatigue and the presence of some macroscopic radial cracks. The numerical thermals model was developed. Two series of seven braking series stopped successively have been simulated, in the case of uniform pressure distribution, and in the case of hot spots. In both cases, numerical results are in accordance with experimental observations. Strength-strain calculated will be applied further in several models of thermal fatigue damage for the prediction of disk life [40].

According to Seo *et al.* [41], a multitude of studies have reported an increase or decrease in the contact fatigue life, as measured by the method of removing material from the contact surface. However, the fundamental mechanisms underlying the changes in fatigue life have not been

comprehensively explored. In the study he carried out, the effect of the depth of removal of metals at the contact fatigue life was evaluated by applying the analysis of elements and conducting appropriate fatigue tests. It has been revealed that the residual stress and stress flow are the main factors that determine the life of fatigue. The railroad wheels have the initial residue stress formed during the manufacturing process, and this residue stress changes due to the thermal stress caused by braking. It has been observed that stress residuals determine the amount of depth of removal of metals for optimal fatigue life. Also, the effect of the residual stress and the removal of metals at the contact fatigue life has been estimated, and the equation is proposed to calculate the optimal depth of metal removal to maximize the contact fatigue life [41].

According to Cristol-Bulthé *et al.* explained that there were several parameters to determine the parameters specified during the testing process on a scale dynamometer machine [42]:

$$\hat{p}\hat{v}_0\sqrt{\hat{t}_f} = \gamma,$$

where $\hat{p}$, $\hat{v}_0$, dan $\hat{t}_f$ are a dimensionless in a row contact pressure, initial velocity, and braking time, respectively; and then $\gamma$ becomes a parametric triplet factor, constant characteristics of the geometry of materials, and specimens. Without dimensional parameters are defined as reduced scale ratios on full-scale values.

$$\hat{p} = \frac{p}{P};\ \hat{v}_0 = \frac{v_0}{V_0};\ \hat{t}_f = \frac{t_f}{T_f}.$$

Here, $p$ is the contact pressure on reduced scale (MPA), $\hat{p}$ is the dimensionless contact pressure, $P$ is the contact pressure on a full scale (MPA), $t$ is time (s), $t_f$ is the duration of stop braking on a reduced scale (s), $\hat{t}_f$ is the dimensionless duration of stop braking, $T_f$ is the duration of stop braking on a full scale (s), $v_0$ is the initial speed in full scale stop braking (m/s), $\hat{v}_0$ is the dimensionless speed initial, $V_0$ is the initial speed in reduced scale stop braking (m/s), and $\gamma$ is the triple factor parameter.

Anders and Elena in 2005 explained the process of forming cracks on the train wheels caused by trapped fluid. This phenomenon is shown in Figure 4. Figure 4 is drawn based on information and the stud by Ekberg and Kabo [43].

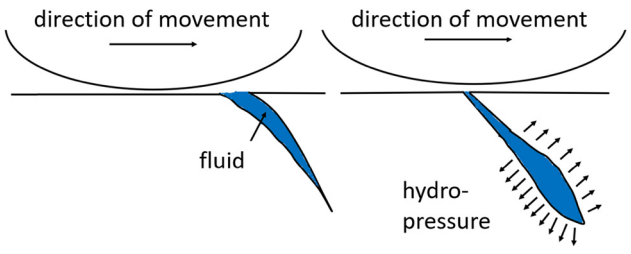


**Figure 4:** The mechanism for the formation of cracks caused by caught fluid [43].

Šamec *et al.* explained the results of their research related to cast iron used as the main ingredient in making brake lining against fatigue resistance in several temperature conditions. Fatigue is checked at room temperature, 300 and 400°C. Modulus Young remains stable enough temperature, while the maximum evidence and tensile strength decreases with increased temperature. Fatigue/fatigue decreased by about 50% at 300°C, while a sample of 400°C only experienced 10% of their strain reversal at temperature [30].

According to Wang *et al.*, brake disc wear is a significant problem in the high-speed railroad system, and the progressive development of fatigue cracks during the braking cycle has been identified as a key contributing factor to the deterioration of braking integrity. The presence of modified microstructures, characterized by a white etching layer containing nano-sized ferrite, was observed on the friction surface of worn brake discs. To analyze how the thermal stress and sequential mechanics affect the cracking of cracks and the evolution of microstructure in brake discs, successive braking cycles are simulated in the full-scale bench test rig. Crack initiation and propagation mechanism are proposed based on the results of experiments, namely, (i) crack initiation and propagation mechanism are proposed based on the results of experiments, namely, thermal crack formation is induced by thermal transients during the braking process; (ii) increased roughness of friction surfaces due to thermal cracks has been shown to induce local stress concentration; (iii) localized frictional stress and thermal stress have been shown to drive the propagation of thermal cracks, which subsequently merge with radial main cracks. Analysis of thermal-mechanical conditions that exist on the friction surface during braking shows that the formation of a white etching layer can be associated with severe plastic deformation caused by repeated friction between discs and bearings. Mechanical testing also shows that the formation of a white etching layer does not harm the integrity of the brake disc [44].

Wu *et al.* explained the relationship between the coefficient of friction ($K_w$), the normal force ($N$), the hardness of a material ($H$), the length of the trajectory ($D$), and the volume of wear ($V_{wear}$) as follows [45]:

$$V_{wear} = k_w \frac{N \cdot d}{H}.$$

According to Makino *et al.* one thing that affects the cracks is the slip ratio. The slip ratio can be calculated using the following equation [46]:

$$S_r = \frac{V_r - V_w}{V_w},$$

**Table 6:** Milestone of failure, accident, and technical loss from the braking/railroad system

| Milestone | Author | Title | Important remarks | Ref |
|---|---|---|---|---|
| 1987 | S. Wise | Railway Wheelsets – A Critical Review | A brief history of the evolution of wheelsets and then outlines the changes that have occurred in their design in the last 30 years, mainly due to changes in diesel and electrical traction | [17] |
| 1988 | A. Martín Meizoso and J. Gil Sevillano | Life Prediction of Thermally Cracked Railway Wheels: Growth Estimation of Cracks with Arbitrary Shape | The estimated method for the prediction of crack growth is used to provide a limit for the front position of instant cracks and estimated cracks in short computing time | [38] |
| 1991 | N. Kumagai, H. Ishikawa, K. Haga, T. Kigawa, and K. Nagase | Factors of Wheel Flats Occurrence and Preventive Measures | Flat wheels, caused by rolling stock braking, do not carry vibrations and noise into the vehicle and also do not cause mechanical damage to the bearing and axles | [35] |
| 1991 | A. J. Day, M. Tirovic, and T. P. Newcomb | Thermal Effects and Pressure Distributions in Brakes | Thermal effects of the interface pressure distribution can be divided into bulk temperature effects, such as the expansion of brake drums and brake discs, and macroscopic thermal effects | [36] |
| 1996 | J. Kalousek, E. Magel, J. Strasser, W. N. Caldwell, G. Kanevsky, and B. Blevins | Tribological Interrelationship of Seasonal Fluctuations of Freight Car Wheel Wear, Contact Fatigue Shelling and Composition Brakeshoe Consumption | A strong relationship between brake shoe metal and appropriate increase in the tread of the wheel and shooting during the winter months | [37] |
| 2002 | P. Dufrénoy, G. Bodovillé, and G. Degallaix | Damage Mechanisms and Thermomechanical Loading of Brake Discs | The mechanism of damage to the railroad disc brakes that lead to macroscopic cracked events on the friction surface | [40] |
| 2005 | Anders Ekberg, and Elena Kabo | Fatigue of Railway Wheels and Rails Under Rolling Contact and Thermal Loading-An Overview | The mechanism behind various phenomena, predictions, influences of parameters and possible ways of prevention on rail wheel defects | [43] |
| 2007 | A. L. Cristol-Bulthé, Y. Desplanques, G. Degallaix | Coupling Between Friction Physical Mechanisms and Transient Thermal Phenomena Involved in Pad-Disc Contact During Railway Braking | Disk wave distortion, giving contact and leads to the formation of three dimensions in the form of a flat plate that stabilizes the friction coefficient | [42] |
| 2008 | U. Zerbst, K. Mädler, and H. Hintze | Fracture Mechanics in Railway Applications – An overview | General introduction to the application of fracture mechanics to the railroad component | [39] |
| 2008 | Jung Won Seo, Byeong Choon Goo, Jae Boong Choi, Young Jin Kim | Effects of Metal Removal and Residual Stress on the Contact Fatigue Life of Railway Wheel | The residual stress and plastic flow are major factors determining the fatigue life | [41] |
| 2011 | B. Šamec, I. Potrč, and M. Šraml | Low Cycle Fatigue of Nodular Cast Iron Used for Railway Brake Discs | Evaluate the fatigue life of nodular cast iron | [30] |
| 2012 | Taizo Makino, Takanori Kato, dan Kenji Hirakawa | The Effect of Slip Ratio on the Rolling Contact Fatigue Property of Railway Wheel Steel | The RCF test results show that cracks begin on the surface, reproduced in a depth and then branched | [46] |
| 2015 | Reza Masoudi Nejad, Khalil Farhangdoost, Mahmoud Shariati | Numerical Study on Fatigue Crack Growth in Railway Wheels Under the Influence of Residual Stresses | Provide predictions of cracked growth on the rail wheels under the influence of the stress from the mechanical load and the heat treatment process of the railroad wheels | [47] |
| 2019 | Z. Wang, J. Han, J. P. Domblesky, Z. Li, X. Fan, and X. Liu | Crack Propagation and Microstructural Transformation on the Friction Surface of a High-Speed Railway Brake Disc | The propagation of cracking fatigue and microstructure transformation on the friction surface of the high-speed rail brake discs were analyzed | [44] |
| 2019 | Xingwen Wu, Subhash Rakheja, Wubin Cai, Maoru Chi, A. K.W. Ahmed, Sheng Qu | A Study of Formation of High Order Wheel Polygonalization | Increasing the damping rail bearings can effectively reduce the growth rate of high-order wheels | [45] |

(*Continued*)

**Table 6:** *Continued*

| Milestone | Author | Title | Important remarks | Ref |
|---|---|---|---|---|
| 2021 | Xie, Xiaodong Li, Zhiqiang Domblesky, Joseph P. Yang, Zhiyong Liu, Xiaolong Li, Weijing Han, Jianmin | Analysis of deep crack formation and propagation in railway brake discs | Crack formation in and unstable growth EMU after two radial in-line cracks are found during routine maintenance inspections | [49] |
| 2021 | Reza Masoudi Nejad, Zhiliang Liu, Wenchen Ma, dan Filippo Berto | Reliability Analysis of Fatigue Crack Growth for Rail Steel Under Variable Amplitude Service Loading Conditions and Wear | Investigate the effect of the condition of loading amplitude service variables and wear and phenomena on reliability analysis for rail steel | [51] |
| 2022 | Y. Yang, L. Ling, C. Wang, Z. Liu, K. Wang, and W. Zhai | Wheel/rail dynamic interaction induced by polygonal wear of locomotive wheels | Investigation of the effects of the Wear Heul's Locomotive Roda on dynamic performance and rail/rail interaction through tests in a broad place and numerical simulation, where special attention is given to locomotive vibrations and the dynamics of the tangential troops/rails | [48] |
| 2023 | C. Lu, J. Shen, Q. Fu, and J. Mo | Research on radial crack propagation of railway brake disc under emergency braking conditions | Emergency braking conditions 270 km/h as an example to analyze the problem of fatigue cracks from the brake disc | [50] |

where $S_r$ is a slip ratio, $V_r$ is the speed of the railroad tracks, and $V_w$ is the speed of the railroad wheels.

Masoudi Nejad *et al.* explained about the development of fatigue in the railroad wheel cracks. In this study, modifying Paris equations determine the rate of fracture and fatigue, which is given as follows [47]:

$$\frac{da}{dN} = C(\Delta K_{\text{eff}})^n = C(K_{\max} - K_{\text{op}})^n ,$$

where $\Delta K_{\text{eff}}$ is an effective stress intensity factor, $K_{\max}$ is the maximum stress intensity factor, and $K_{op}$ is the level of the stress where the first crack occurs. $C$ and $n$ are the same material constant as $C = 3.38 \times 10^{-12}$ m/cycle and $n$ equals to 3.

According to Yang *et al.*, seriously polygonal tear usually causes a drastic wheel/rail interaction, which threatens the safety of the railroad vehicle. A research investigation was conducted to examine the impact of polygonal wear on heavy-haul locomotive wheels on the dynamic performance and wheel/rail interactions. This investigation involved extensive on-site tests and numerical simulations, with a particular focus on locomotive vibrations and dynamic wheel/rail tangential forces. The results measured by the first two objective locomotives are compared, including the characteristics of the polygonal wear of the wheels and locomotive vibrations in the vertical, longitudinal, and lateral directions. The 3D train dynamic model is combined and then formulated to investigate the dynamic interaction of the wheel/rails caused by the polygonal wear of the locomotive wheel. Low adhesion zone and PI-based antislip control algorithms are embedded into a dynamic model to analyze the effects of polygonal wheels in longitudinal and lateral/rail/rail interactions under normal and low adhesion conditions. The results show that severe polygonal wear affects not only vertical but also the longitudinal performance of the wheel/rail system mainly [48].

Xie *et al.* examined the steel brake discs were analyzed after the cracks were found during the maintenance examination. The aim is to identify encouragement for typical semi-ellipse cracking. Element to expanded methods that include residual stress effects of services are used to analyze the history of thermo-mechanical and cracking produced. Actual fracture surfaces show a satisfying agreement and indicate that special cracks begin in the corner of the bolt hole and temporary temperature differences between adjacent hot spots help determine the orientation of cracks. It was also found that unstable propagation along the axial direction was caused by a steep temperature gradient. Distortion-induced services is also found to show internal pressure that can have a strong effect on cracking behavior. It is hoped that the findings will contribute to a better understanding of how braking conditions and service effects affect

**Table 7:** Accident rates on trains in Japan [52–58]

| Year | The number of cases | | | | |
|---|---|---|---|---|---|
| | Railroad accident | Accident on the crossing path | Accident with casualties | Accident with material damage | Total railroad accident cases each year |
| 2016 | 1 | 37 | 144 | 0 | 182 |
| 2017 | 0 | 39 | 138 | 0 | 177 |
| 2018 | 0 | 42 | 118 | 0 | 160 |
| 2019 | 0 | 37 | 118 | 0 | 155 |
| 2020 | 1 | 29 | 107 | 0 | 137 |
| 2021 | 2 | 24 | 90 | 0 | 116 |
| 2022 | 2 | 41 | 73 | 2 | 118 |

unstable crack behavior on electric multiple unit (EMU) brake discs [49].

Lu *et al.* also explained that fatigue damage from brake discs significantly affected the safety of railroad braking. Research conducted by Lu took an emergency condition of 270 km/h as an example to analyze the problem of fatigue cracks from the brake disc. A theoretical analysis and simulation of elements pertaining to thermo-mechanical processes have been instrumental in elucidating the cracking behavior of the brake disc, which exhibits a radial directionality. A thorough investigation has been conducted to ascertain the crack threshold, fracture toughness, and length of the designated brake disc. The results showed that the growth rate of brake disc cracks followed the radial direction greater than the direction of thickness. However, because the thickness dimension is much smaller than the radial dimension, cracking of cracks along the thickness direction can cause cracks to crack through thickness, and unstable propagation will occur when the cracked length reaches 60 mm [50].

Masoudi Nejad *et al.* explained the equation of cracking cracks using the following equation [51]:

$$\frac{\mathrm{d}a}{\mathrm{d}N} = f_I(\Delta K, R),$$

where $\Delta K$ is the range of the intensity factor of the stress then $R$ is the load ratio. Table 6 illustrates milestone of failure, accident, and technical loss from the braking/railroad system.

# 4 Financial loss due to a braking accident/railroad system

A company is “East Japan Railway Company,” which is engaged in the main passenger train in Japan. The company is officially abbreviated as JR-east and as JR Higashi-Nihon in Japanese. In general, accidents that occurred in Japan in the period from 1988 to 2022 were volatile. Starting from 1988 to 2007, the railroad accident rate tends to fall later in 2008 to 2015, then increase from 2016 to 2022, and then continued to fall. When compared between 1988 and 2022, 2022 experienced a very significant decline. In 1988, there were 376 cases of accidents, while in 2022, only 118 cases meant had decreased to 70%. In detail, the accident rate can be seen in Table 7 from 2016 to 2022 [52].

In Table 7, we can see during the last 7 years the total case of train accidents each year tends to decrease. Only in 2022 show an increase of two cases when compared to the previous year. The biggest presentation of the case that arises in the train accident in the category of accidents with casualties. Accidents with casualties include people who were hit by a train either died or injured, but not including people who committed suicide.

In the European Union, there is a body in charge of setting public safety targets, general safety methods, and general safety indicators namely “European Union Agency for Railways” or often abbreviated (era). In recent years, the era records losses resulting from train accidents. The following data are related to the cost of losses generated due to train accidents in Europe (Figure 5 and Table 8). Figure 5 is drawn based on information and the previous studies [59–62].

Based on the data in 2018, there is a significant increase even 200% from 2016. This is due to a very significant increase in the cost of fatal events. Then in 2020 decreased, especially in the group of fatal events, decreased to 23%. This is because not all countries in Europe are recorded and reported. This is evidenced by the accident rates that exist over the past few years shown in Figure 6. The accident rates that have been recorded tend to decline in recent years. Figure 6 is drawn based on information and the study by European Union Agency for Railways [62].

An independent company, “Office of Rail and Road,” works in the field of transportation, especially in the field of railroads and highways in the United Kingdom. Every

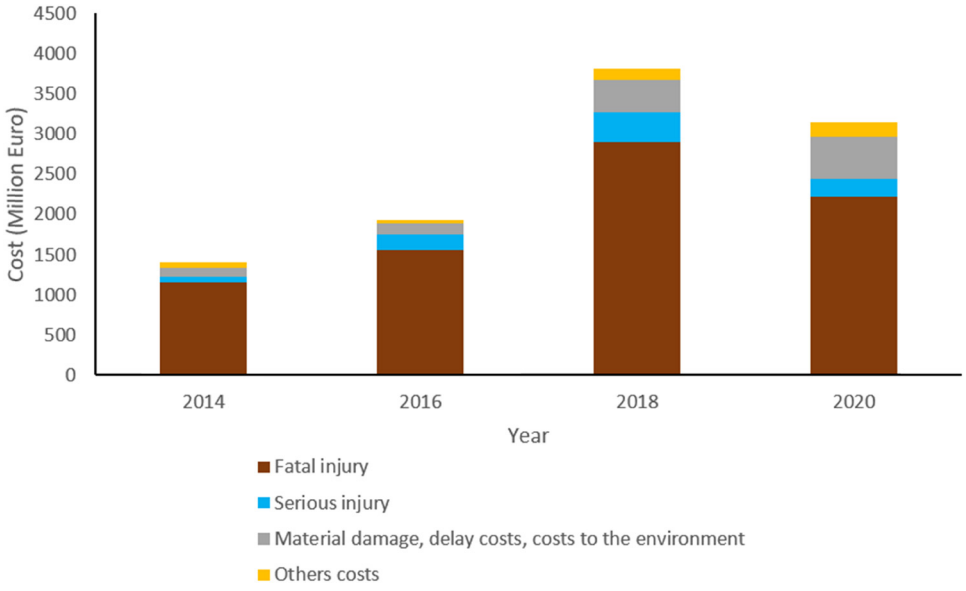


**Figure 5:** The graph of the loss costs caused by a train accident in Europe [59–62].

**Table 8:** Cost Details caused by accidents on trains in Europe [59–62]

| Year | Fatal injury | Serious injury | Material damage, delay costs, costs to the environment | Other costs | Total |
|---|---|---|---|---|---|
| 2014 | 1,155 | 71 | 103 | 71 | 1,400 |
| 2016 | 1,559 | 192 | 141 | 37 | 1,929 |
| 2018 | 2,897 | 379 | 393 | 142 | 3,811 |
| 2020 | 2,221 | 228 | 520 | 187 | 3,156 |

year, the Office of Rail and Road records cases related to safety factors on the train. This includes the number of deaths and injuries that affect labor, nonlabor (passengers and other community members), and intruders in various railroad networks. It also includes incidents in the crossing path, information about train accidents, and signals that are passed on danger. The existing data are presented in Figure 7 and Table 9. Figure 7 is drawn based on information and previous studies [63–66].

Based on the aforementioned data in the United Kingdom, accident cases are grouped into three of them, Mainline Rail Network, London Underground, Trams, metros, and other nonnetwork rail networks. The Mainline Rail Network group is a case that appears on the main route of the train that is run and managed by "Rail Network." The scope is limited to cases that occur at the station, trains or infrastructure that are still managed by "Rail Network." The

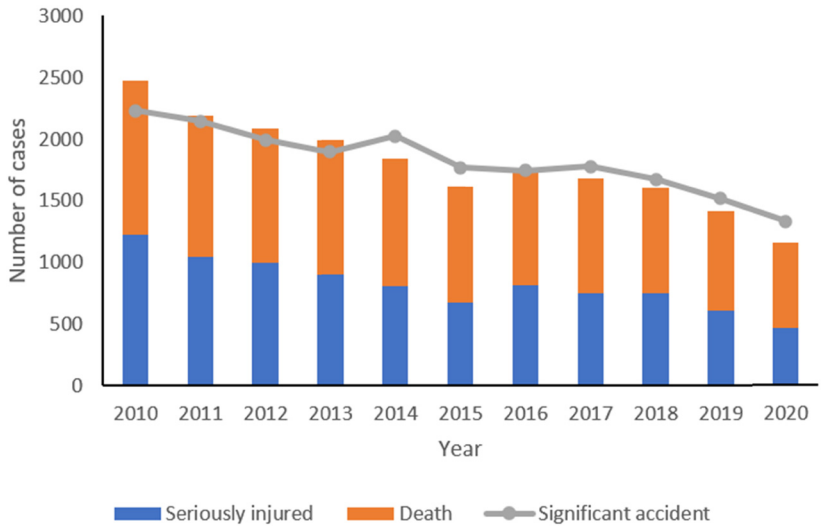


**Figure 6:** Graphics of accidents on train in Europe [62].


**Figure 7:** Accident events on trains in the United Kingdom [63–66].

London Underground group or often also called "tube" is a case that appears on the path operated by "London Underground Limited, which is owned by Transport for London." The last group of Trams, Metros and Other Non-Network Rail Networks includes cases that occur in Terms operators, Non-Main Network Railroad Systems [63–66].

Data over the past 9 years shown in Figure 7 show an increase and a decrease that tends to be random. But if we compare the last two periods in the period 2020–2021 with 2021–2022, the number of accident cases tends to increase quite dramatically 32%.

**Table 9:** Railroad accident rates in the United Kingdom [63–66]

| Year | The number of cases | | | |
|---|---|---|---|---|
| | Mainline rail network | London underground | Trams, metros, and other nonnetwork rail networks | Total |
| 2013–2014 | 454 | 20 | 24 | 498 |
| 2014–2015 | 438 | 11 | 110 | 559 |
| 2015–2016 | 415 | 11 | 143 | 569 |
| 2016–2017 | 350 | 15 | 123 | 488 |
| 2017–2018 | 314 | 14 | 112 | 440 |
| 2018–2019 | 360 | 24 | 133 | 517 |
| 2019–2020 | 408 | 28 | 98 | 534 |
| 2020–2021 | 285 | 5 | 71 | 361 |
| 2021–2022 | 343 | 7 | 126 | 476 |

# 5 Advanced material for the development of braking design/ train driving system

The material from the rail brake block in the period before the millennial period was studied by Mercer in 1987. The study explained nonmetal material as a substitute for cast iron material in brake lining. This composite brake lining exhibits superior qualities, including enhanced durability and resistance to wear. Research conducted by Mercer was conducted at the "Central Railway of Peru" [16]. The route traversed in this area is characterized by a series of zig-zags, descending downhill. The incidence of flattening wheels often occurs due to the substandard quality of brake blocks that produce excess friction.

A research study was conducted to ascertain whether the composite brake block has the capacity to replace the cast iron brake block. To this end, several test methods were employed [16]. Wear testing is carried out with the stop test method at a speed range of 16–144 km/h braking force of 2,000 and 6,000 lbf. Then the second gradient test method is carried out with a duration of 45 min braking force 925 and 1,450 lbf. The results obtained are shown in Table 10.

Research conducted by Chen *et al.* examined the addition of aluminum to the Cu-Fe-C material. Aluminum is an important alloy element that is often added to iron-based

**Table 10:** Comparison of wear cast iron brake with composite X627 [16]

| Material type | Stop test (loss in volume) | Grade test (loss in volume) |
|---|---|---|
| Cast iron | 1.32 $in^3$ | 2.03 $in^3$ |
| Composite X627 | 0.24 $in^3$ | 0.25 $in^3$ |

**Table 11:** Composition of material that is varied [67]

| Specimen code | Copper | Steel wool | Graphite | Aluminum | Alumina | Tin |
|---|---|---|---|---|---|---|
| A0 | 50 | 10 | 20 | 0 | 10 | 10 |
| A10 | 40 | 10 | 20 | 10 | 10 | 10 |
| A20 | 30 | 10 | 20 | 20 | 10 | 10 |

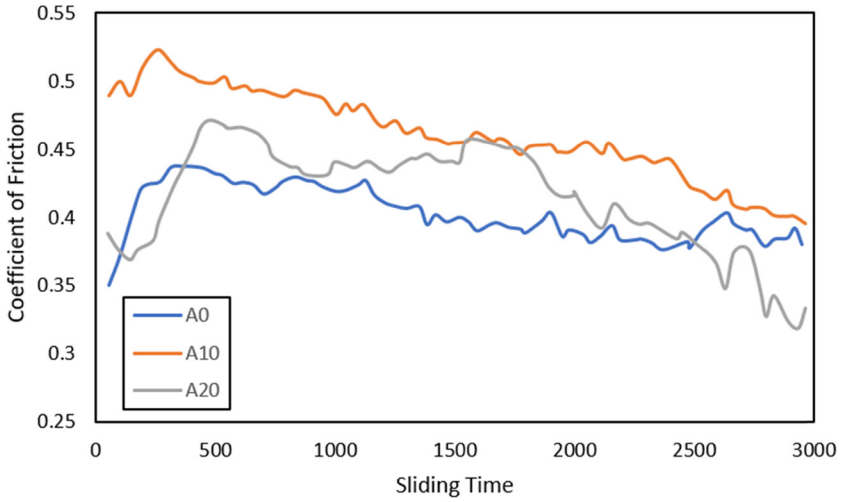


**Figure 8:** Average variations in friction coefficient with sliding time [67].

friction material [67]. In research conducted by Chen, the composition of the material that was varied is presented in Table 11. Table 11 shows the composition of the constituent particles by volume fraction when copper is used as a compensation material.

The manufacturing process begins by mixing all the materials, then continues with compaction and sintering. The material that has been undergoing the sinter process is carried out testing the coefficient of friction and also calculates the mass lost. From these tests obtained data as in Figure 8 and Table 12. Figure 8 is drawn based on information and the study by Chen *et al.* [67]. The results of friction tests conducted in the three variations show that the A10 variation shows the highest and most stable coefficient compared to the three variations. While the results of the missing mass testing sample A10 into material show the least decrease in mass. The friction and wear data clearly shows the superiority of the A10/FC30 combination in tribology performance compared to two other combinations (A0/FC30 and A20/FC30) [67].

Other studies conducted by Chen *et al.* examined the effect of the addition of graphite on the Cu-Fe-C material. Graphite is a material that can affect the coefficient of friction and the rate of wear of the material with the main structure of iron. This is because graphite provides benefits to the sinter process [68]. In the research conducted by Chen, the composition of the material that was varied is shown in Table 13. Table 13 shows the composition of the constituent particles by volume fraction when copper is used as a compensation material.

The material undergoes the mixing process, then the compact process, and finally the sinter process. The material that has been undergoing the sinter process is carried out testing the coefficient of friction and also calculates the mass lost. From these tests, obtained data are shown in Figures 9 and 10. Figures 9 and 10 are drawn based on

**Table 12:** Mass loss (g) of Cu–Fe–C and FC30 after wear [67]

| Specimen code | A0 | FC30 (VsA0) | A10 | FC30 (VsA10) | A20 | FC30 (VsA20) |
|---|---|---|---|---|---|---|
| Weight loss | 0.034 ± 0.012 | 0.081 ± 0.032 | 0.006 ± 0.002 | 0.070 ± 0.014 | 0.063 ± 0.033 | 0.096 ± 0.064 |

**Table 13:** Composition of material that is varied [68]

| Specimen code | Copper | Steel wool | Graphite | Aluminum | Alumina | Tin |
|---|---|---|---|---|---|---|
| C0 | 60 | 10 | 0 | 10 | 10 | 10 |
| C10 | 50 | 10 | 10 | 10 | 10 | 10 |
| C20 | 40 | 10 | 20 | 10 | 10 | 10 |

information and the study by Chen *et al.* [68]. The results of the friction coefficient testing on the C0 and C10 samples have the same friction behavior, both decreased from time to time. However, the C20 sample maintains a high and stable friction coefficient during testing.

During the friction test, data were also obtained from the reduction of the lost mass of each sample tested on the FC30 disk. In testing with variations in the C0 and C10 samples, the FC30 disk that lost a lot of mass was caused by the layer of the film formed attached to the surface either C0 or C10. Conversely, the C20 variation exhibits a greater mass loss due to its lower hardness and density. Consequently, the powder formed adheres more readily to the FC30 disk.

Still in the same year, Ghaderi *et al.* examined the influence of graphite morphology on austempered cast iron from the tribology side. This study uses three types of cast iron with different graphite morphology, namely,

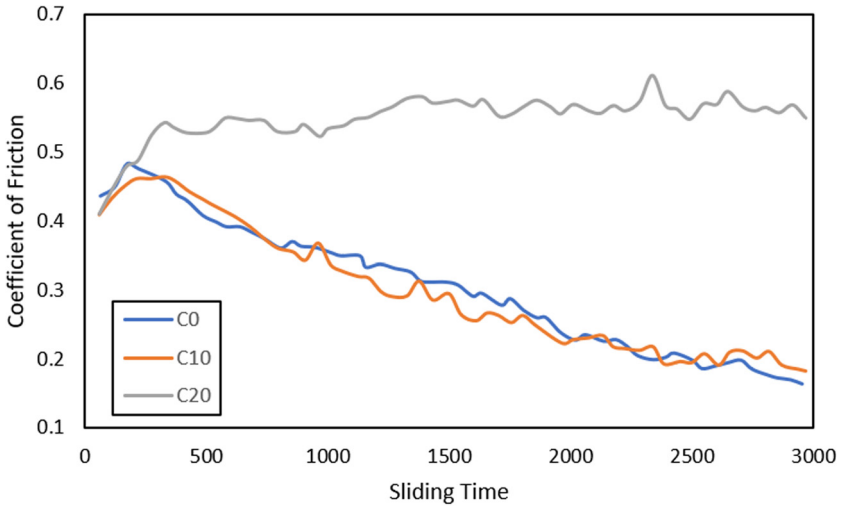


**Figure 9:** Typical variations in friction coefficient with sliding time [68].

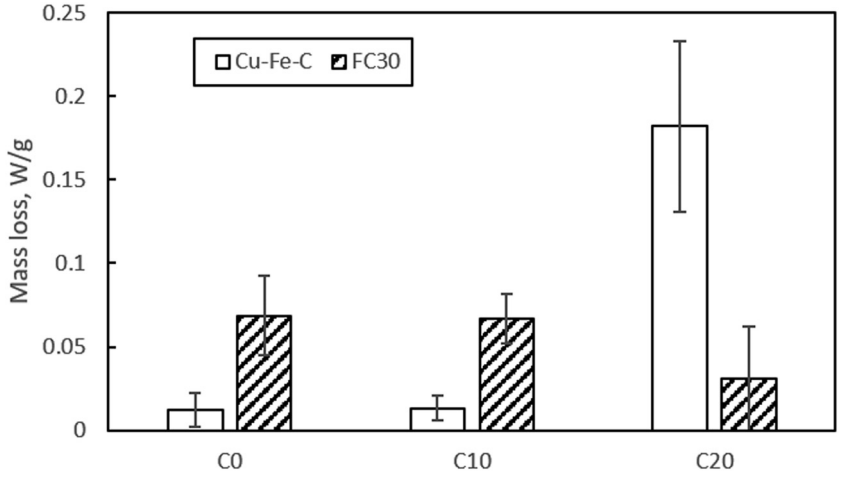


**Figure 10:** Mass losses of Cu-Fe-C and FC30 after sliding for 3,000 s [68].

**Table 14:** Chemical composition (wt%) and graphite morphology of specimens [69]

| Specimens | Type | C | Si | Mn | Ni | Mo | Cu | Ti | Mg | P | Fe |
|---|---|---|---|---|---|---|---|---|---|---|---|
| G1 | Gray | 3.27 | 2.19 | 0.26 | 1.00 | 0.18 | 0.56 | — | — | — | Balance |
| G2 | Gray | 3.46 | 2.02 | 0.32 | 1.12 | 0.30 | 0.61 | — | — | — | Balance |
| C1 | Compact | 3.20 | 2.50 | 0.50 | 0.40 | 0.08 | 0.68 | 0.12 | 0.025 | — | Balance |
| C2 | Compact | 3.45 | 2.11 | 0.18 | 0.90 | 0.20 | 0.60 | 0.08 | 0.02 | — | Balance |
| D1 | Ductile[a] | 3.23 | 2.43 | 0.33 | 1.05 | 0.22 | 0.60 | — | 0.04 | — | Balance |
| G3 | Gray | 3.30 | 2.10 | 0.50 | — | — | — | — | — | 0.9 | Balance |

[a]Nodular iron.

gray iron, nodular iron, and compact iron. The chemical composition of several types of cast iron used is displayed in Table 14. The three types of cast iron were each subjected to an austempered treatment, and the friction coefficient was subsequently determined through testing. The lost mass was also calculated and is illustrated in Figures 11–13. Figures 11–13 are drawn based on information and the study by Ghaderi *et al.* [69].

From the research conducted, the nodular austempered cast iron has the highest impact resistance, while the gray cast iron has lowest impact resistance. Austempered nodular and gray cast iron has lower wear resistance than austempered compact cast iron. The overall resistance of austempered cast iron is better than pearlitic gray iron, especially at lower friction speeds [69].

Research conducted by Hirasata examined the characteristics of friction and wear of some cast iron under certain conditions and pressures. In Table 15, the chemical composition of each cast iron used [70].

From the research conducted, the friction coefficient of each cast iron approaches the constant value as an increase in shear distance, and this value does not depend on contact pressure but decreases with an increase in friction speed.

Research conducted by Ertan and Yavuz used the composition of the compilers of the Automotive and Brake

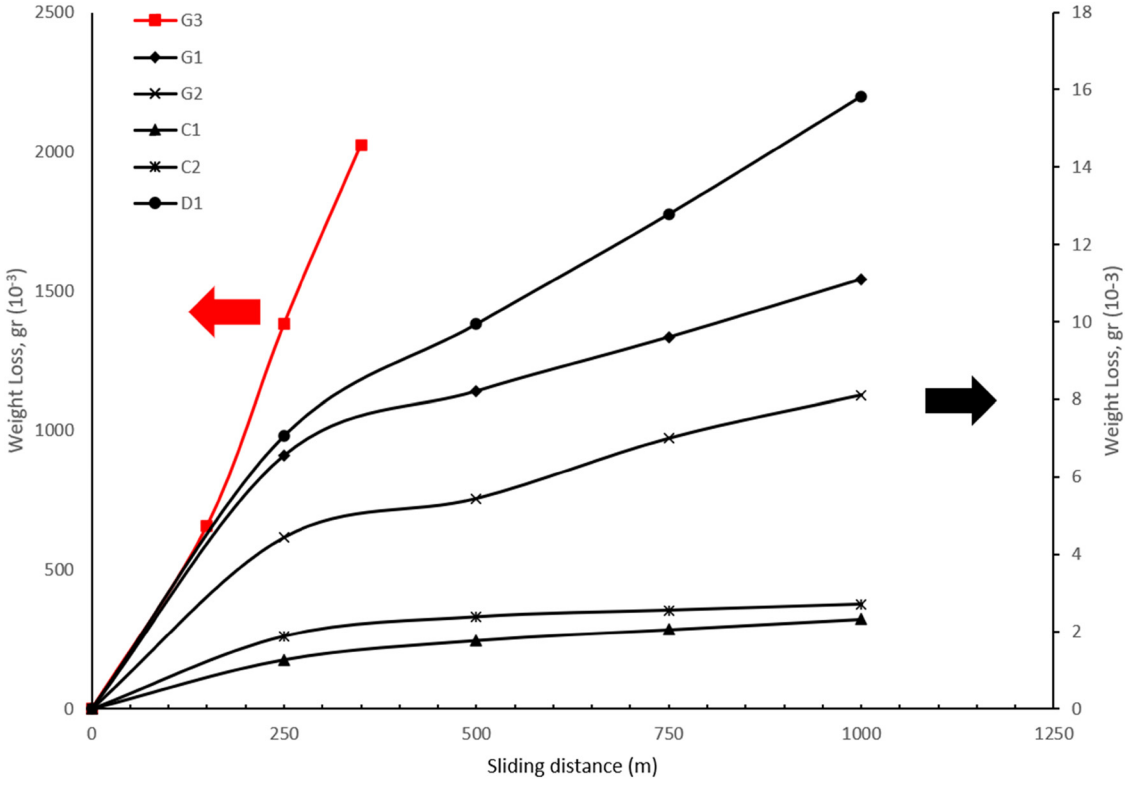


**Figure 11:** Weight loss *vs* sliding distance of austempered specimens at an applied load of 90 N and running speed of 250 rpm [69].

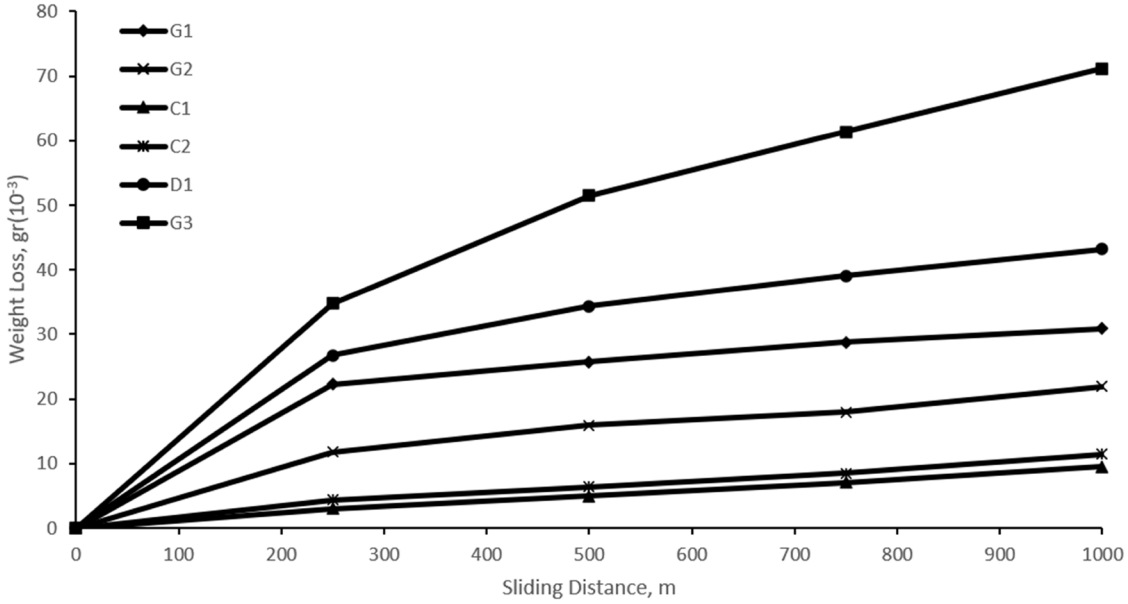


**Figure 12:** Weight loss *vs* sliding distance of austempered specimens and pearlite gray iron when $F$ = 90 N and $v$ = 950 rpm [69].

Lining Industry Corporation. The percentage of each material used is displayed in Table 16 is then optimized through several stages, including the optimization of the reinforcement material, then the optimization of the lubricant's material, and with the optimization of abrasive material.

The friction coefficients and wear rates of the materials examined by Ertan and Yavuz (Table 16) were subsequently analyzed, and the results are presented in Figure 14. Figure 14 is drawn based on information and the study by Ertan and Yavuz [71]. This initial formula is then tested and produces a friction coefficient value of 0.35 (for temperature <250°C) and 0.32 (for temperature >250°C). Its wear rate is 1.95 × $10^{-7}$ $cm^3$/nm [71].

Material reinforcements (copper powder, aramid pulp, rockwool) play a role in increasing the coefficient of friction (CoF) and friction stability, but increases the rate of wear. Materials lubricants (Graphite, Coke, ZnS) also play a role in the increase in the coefficient of friction but reduce the rate of satisfaction. Material abrasives ($ZrSiO_4$, $Fe_2O_3$, cashew dust) not only increases the value of frictional

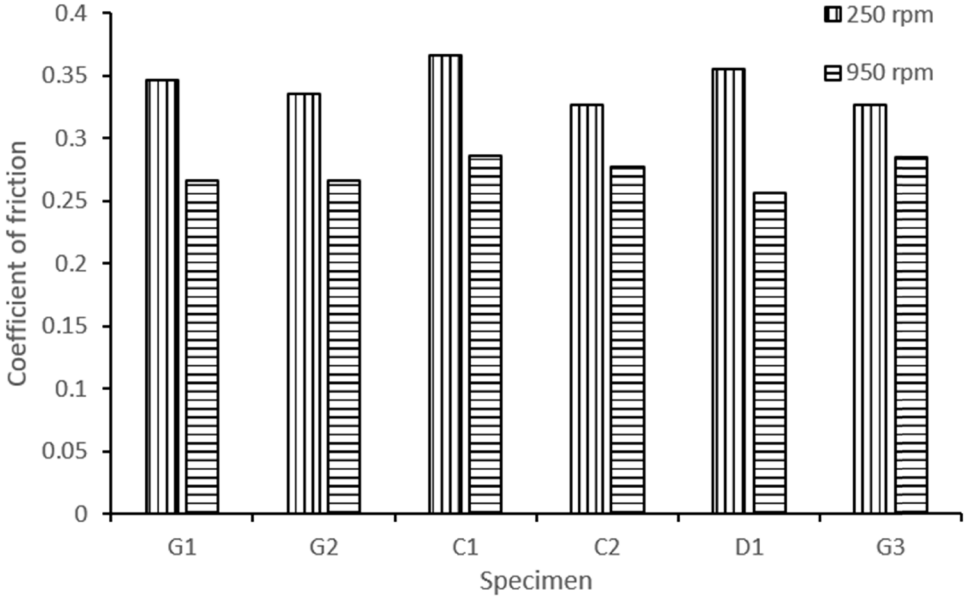


**Figure 13:** Friction coefficient at an applied load of 90 N and running speeds of 250 and 950 rpm [69].

**Table 15:** Chemical components of material [70]

| Material | Pin | | | | | Disk |
|---|---|---|---|---|---|---|
| | FC250 | FC410 | FCD350 | FCD800 | FCAD1200 | SS400 |
| Composition (wt%) | | | | | | |
| C | 3.420 | 3.670 | 3.630 | 3.880 | 3.540 | 0.140 |
| Si | 2.900 | 2.460 | 2.580 | 2.800 | 2.570 | 0.230 |
| Mn | 0.610 | 0.500 | 0.330 | 0.110 | 0.330 | 0.610 |
| P | 0.100 | 0.022 | 0.071 | 0.020 | 0.073 | 0.011 |
| S | 0.010 | 0.005 | 0.012 | 0.007 | 0.012 | 0.005 |
| Mg | — | 0.015 | 0.033 | 0.039 | 0.035 | — |
| Fe | Less | Less | Less | Less | Less | Less |

**Table 16:** Formulation (% wt) of the friction [71]

| Constituents | | Content (% wt) |
|---|---|---|
| Reinforcements | Copper powder | 25 |
| | Rockwool | |
| | Aramid pulp | |
| Binders | Phenolic resin | 10 |
| | Rubber (SBR) | |
| Lubricants | Graphite | 20 |
| | Coke | |
| | ZnS | |
| Abrasives | $ZrSiO_4$ | 15 |
| | $Fe_2O_3$ | |
| | Cashew dust | |
| Fillers | $BaSO_4$ | 30 |
| | $Ca(CO)_3$ | |
| | Wollastonite | |

coefficient but also decreases from the specific rate of material [71]. The composition of the material that has been optimized is displayed in Table 17.

**Table 17:** Composition of optimized materials [71]

| Constituents | | Content (% wt) |
|---|---|---|
| Reinforcements | Copper powder | 6.75 |
| | Rockwool | 14.25 |
| | Aramid pulp | 3.5 |
| Binders | Phenolic resin | 10 |
| | Rubber (SBR) | |
| Lubricants | Graphite | 9 |
| | Coke | 9 |
| | ZnS | 2 |
| Abrasives | $ZrSiO_4$ | 5.1 |
| | $Fe_2O_3$ | 3.45 |
| | Ceshew dusr | 6.45 |
| Fillers | $BaSO_4$ | 30 |
| | $Ca(CO)_3$ | |
| | Wollastonite | |

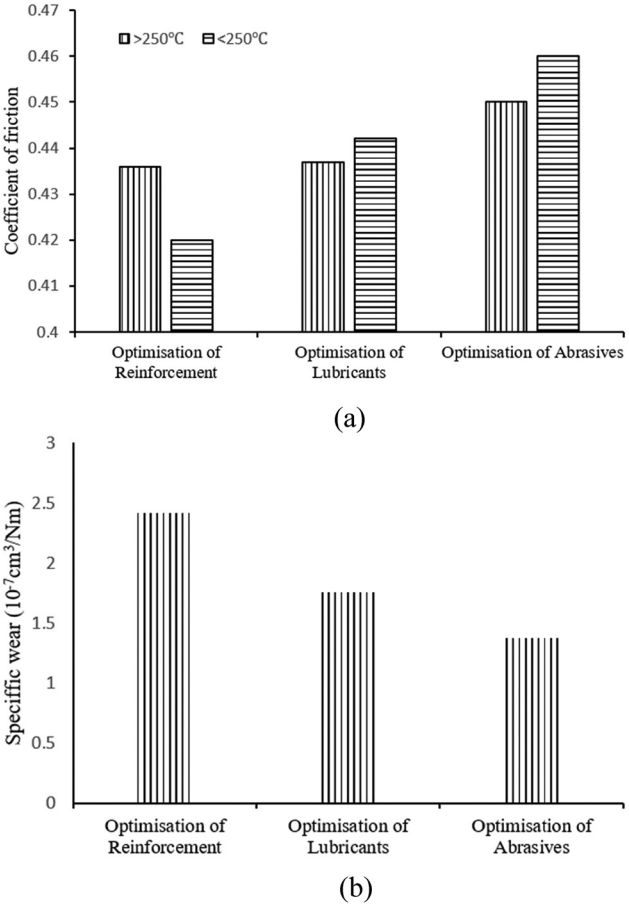


**Figure 14:** Comparisons of (a) CoF (up and under from 250°C) and (b) specific wear rate ($10^{-7}$ $cm^3$/Nm) [71].

Arjmand's research examined rubber-based friction materials (RBFMS) that had been augmented with steel powder and aramid powder to ascertain their tribological properties. Table 18 presents the volume fraction used in each variety [72].

**Table 18:** Composition of brake block [72]

| Ingredients | RM | Comp 1 | Comp 2 |
|---|---|---|---|
| Polymer component | | | |
| SBR 1502 | 0.42 | 0.418 | 0.408 |
| Phenolic resin | 0.082 | 0.080 | 0.078 |
| Rubber curing agents | 0.029 | 0.029 | 0.028 |
| Fillers | | | |
| Fiber | 0 | 0.075 | 0.15 |
| Coal powder | 0.24 | 0.229 | 0.21 |
| Calcium carbonate | 0.072 | 0.058 | 0.043 |
| Iron powder | 0.014 | 0.012 | 0.0086 |
| Barite | 0.070 | 0.056 | 0.042 |
| Iron oxide (magnetite) | 0.033 | 0.026 | 0.02 |
| Iron oxide (limonite) | 0.019 | 0.016 | 0.012 |

**Table 19:** Properties of composites friction materials [72]

| Properties | HRX | Compression modulus (MPa) | Density (g/cm$^3$) |
|---|---|---|---|
| RM | 29.3 (2.5) | 754 (43) | 1.74 |
| SW 7.5% | 18.8 (2.1) | 431 (35) | 2.12 |
| SW 15% | 13 (1.8) | 545 (38) | 2.50 |
| AR 7.5% | 42.8 (4.1) | 795 (40) | 1.65 |
| AR 15% | 52.5 (3.7) | 1,335 (60) | 1.56 |

Variations of comp 1 and comp 2 each has been given the addition of steel powder and aramid powder at 7.5 and 15%, respectively. The results are presented in Table 19.

The results of the friction coefficient and wear rate tests indicated that the addition of steel powder increased the CoF and enhanced friction recovery at low concentrations (7.5 vol%). Conversely, at elevated concentrations (15 vol%) and under conditions of severe friction (abrasive mechanism), the incorporation of steel powder has been observed to result in a decline in CoF, an enhancement of friction, and an increase in wear rate [72].

Shojaei *et al.* [73] examined the RBFMS with the addition of carbon fibers and cellulose fibers to find out the nature of the tribology. The formula of each material to be tested is displayed in Table 20.

Each sample was tested to find out the influence of the addition of carbon fiber and cellulose fiber. Obtained carbon fiber breakdown does not affect the coefficient of friction, while the addition of cellulose fiber is sufficient to affect the addition of the friction coefficient (Tables 21 and 22). When viewed from the wear resistance, the addition of carbon fiber increases the resistance performed in Figure 15. Figure 15 is drawn based on information and reference [73].

Research conducted by Cui *et al.* [74] analyzed the influence of the addition of alumina and graphite on the bronze matrix on the characteristics of friction in the condition of seawater. The formula of each sample to be tested is displayed in Table 23.

Each material is tested at various loading conditions (30, 40, 50, and 60 N) and also the friction speed (0.050, 0.083, 0.116, and 0.150 m/s). From each test, the coefficient of friction and the rate of wear of each sample are shown

**Table 20:** Composition of friction material [73]

| Composite | Polymer component[b] (vol%) | Filler[c] (vol%) | Fiber (vol%) |
|---|---|---|---|
| RM[a] | 0.53 | 0.47 | 0 |
| Comp 1 | 0.53 | 0.395 | 0.075 |
| Comp 2 | 0.53 | 0.32 | 0.15 |

[a]RM: friction material without any fiber.
[b]Polymer component includes SBR 1502 plus curing agent including sulfur, accelerator, zinc oxide and stearic acid (45 vol%) and phenolic resin (8 vol%).
[c]Filler includes coal powder, calcium carbonate, iron powder, barite, and iron oxide.

**Table 21:** μ and μ-recovery *vs* sliding velocity at temperature cycle of 150–350–150°C [73]

| Sliding velocity (rpm) | Material | | | | |
|---|---|---|---|---|---|
| | RM | CAR 7.5% | CAR 15% | CELL 7.5% | CELL 15% |
| 300 rpm | | | | | |
| μ | 0.24 | 0.27 | 0.24 | 0.31 | 0.36 |
| μ-Recovery (%) | 92 | 97 | 89 | 92 | 91 |
| 500 rpm | | | | | |
| μ | 0.24 | 0.28 | 0.25 | 0.32 | 0.34 |
| μ-Recovery (%) | 97 | 110 | 114 | 100 | 100 |
| 700 rpm | | | | | |
| μ | 0.25 | 0.29 | 0.25 | 0.33 | 0.34 |
| μ-Recovery (%) | 102 | 117 | 115 | 108 | 107 |

**Table 22:** μ and μ-recovery at different temperature cycle tested at 700 rpm [73]

| Temperature | Material | | | | |
|---|---|---|---|---|---|
| | RM | CAR 7.5% | CAR 15% | CELL 7.5% | CELL 15% |
| 100°C (100–350–100°C) | | | | | |
| μ | 0.26 | 0.30 | 0.28 | 0.35 | 0.38 |
| μ-Recovery (%) | 97 | 115 | 115 | 94 | 95 |
| 150°C (150–350–150°C) | | | | | |
| μ | 0.25 | 0.29 | 0.25 | 0.33 | 0.34 |
| μ-Recovery (%) | 102 | 117 | 115 | 108 | 107 |
| 200°C (200–350–200°C) | | | | | |
| μ | 0.21 | 0.25 | 0.24 | 0.21 | 0.3 |
| μ-Recovery (%) | 111 | 120 | 116 | 120 | 138 |

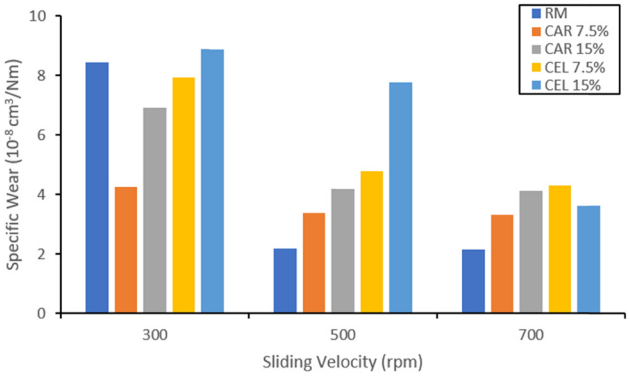


**Figure 15:** Specific wear rate of friction materials *versus* a sliding velocity processed at temperature cycle of 150–350–150°C [73].

**Table 23:** Chemical composition of sintered composites in weight percent [74]

| Specimens | Tin bronze powder (mass%) | Alumina (mass%) | Nickel-coated graphite (mass%) |
|---|---|---|---|
| B1 | 100 | | |
| B2 | 97 | 3 | |
| B3 | 94 | 3 | 3 |

in Figures 16–19. Figures 16–19 are drawn based on information and the study by Cui *et al.* [74].

The addition of alumina is able to increase the coefficient of friction and the wear resistance. Then the sample of the addition of alumina and graphite can reduce the coefficient of friction but still maintains the wear resistance, so that this sample shows the best nature when compared to other samples.

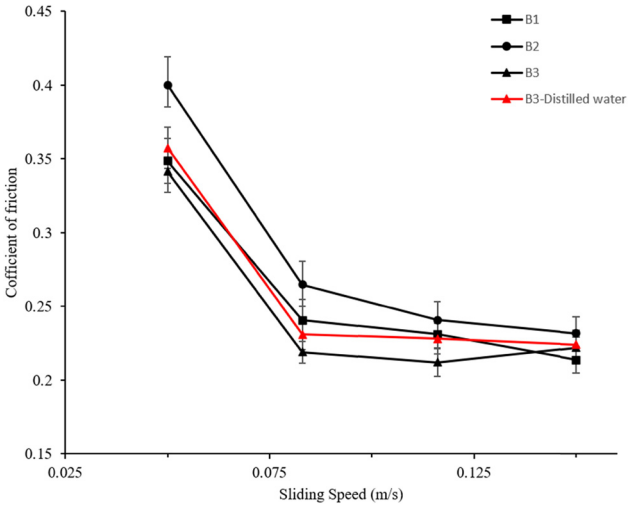


**Figure 17:** Variations of friction coefficient of specimens of specimens with sliding speed at an applied load of 40 N in sea water (black) and distilled water (red) [74].

Surojo *et al.* observed the phenomenon that was due to the proportion of phenolic resins and also fly ash on brake block composites. The formula used for each sample is shown in Table 24 [75].

Each sample was tested for the coefficient of friction using the pin-on-disk method by varying the disk rotary speed (5, 10, 15 m/s) and contact pressure (1; 1.75; 2.5 MPa). The friction coefficient is shown in Figures 20 and 21.

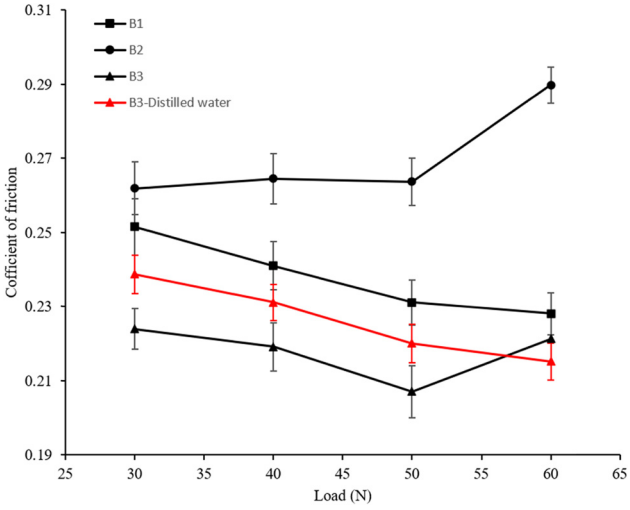


**Figure 16:** Variations of friction coefficient of specimens with applied load at a sliding speed of 0.083 m/s in sea water (black) and distilled water (red) [74].

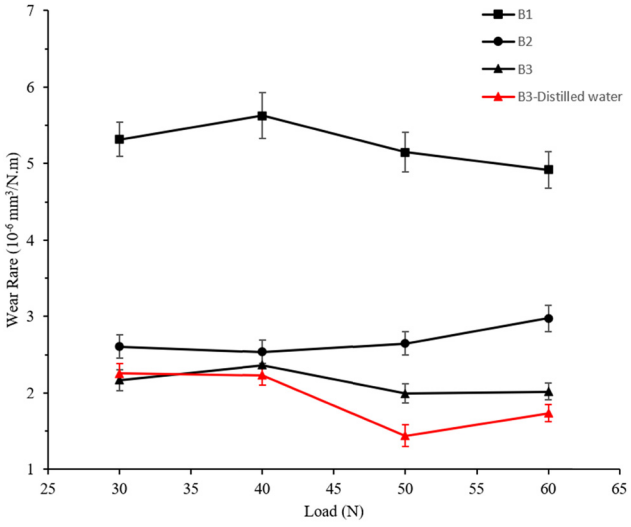


**Figure 18:** Variations of specific wear rate of specimens with applied load at a sliding speed of 0.083 m/s in sea water (black) and distilled water (red) [74].

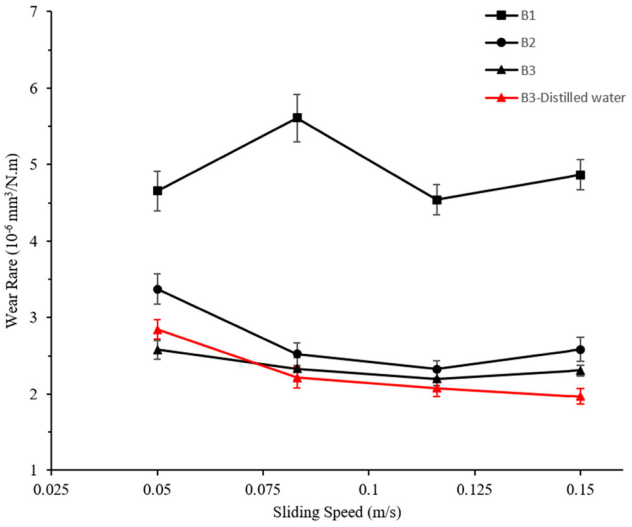


**Figure 19:** Variations of specific wear rate of specimens with sliding speed at an applied loaf of 40 N in sea water (black) and distilled water (red) [74].

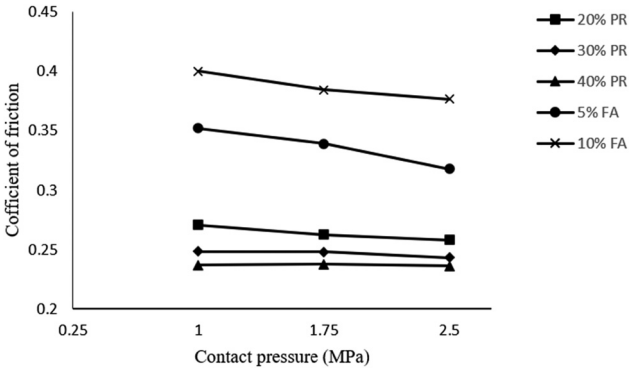


**Figure 20:** Coefficient of friction toward variation of contact pressure with sliding speed 5 m/s [75].

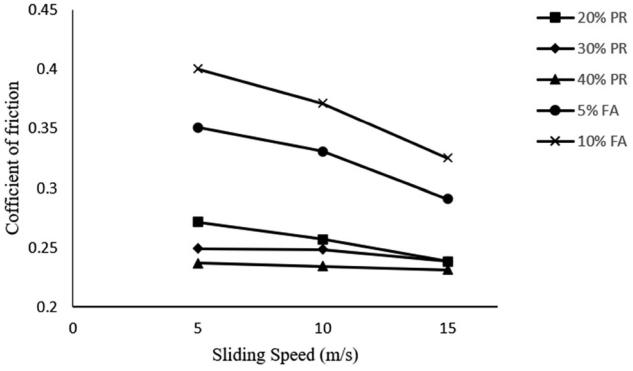


**Figure 21:** Coefficient of friction toward variation of contact pressure with contact pressure 1 MPa [75].

Figures 20 and 21 are drawn based on information and the study by Surojo *et al.* [75].

From the data displayed in Figures 20 and 21, the addition of the percentage of phenolic resins will reduce the coefficient of friction, while the addition of the fly ash will increase the coefficient of friction. Phenolic resin affects the contact and rotary speed of the disc, while the fly ash does not have an impact [75].

Surojo *et al.* [76] this time examined the addition of metallic elements to the composite brake block. The metallic element used by cast iron chip and Cu short wire. The formula used in this study is shown in Table 25.

Each sample is then tested using a tribometer pin on disc with a variation of contact pressure (1; 1.75; 2.5 MPa) and variations of disc rotting speed (5, 10, 15 m/s). The results of the friction coefficient testing are shown in Figure 22 and 23. Figures 22 and 23 are drawn based on information and the study by Surojo *et al.* [76]. The adding of cast iron flakes and copper wire has been demonstrated to enhance the coefficient of friction of the brake pad. This happens because the material forms contacts that strengthen the friction. However, copper wire that is parallel to the direction of friction tends to be separated from the matrix [76].

Li and Yan [77] in 2015 compared three types of brake blocks including brake C/C, C/C-SIC, and metallic to determine the efficiency of friction and the rate of brake block wear on high-speed rails. The braking pressure used is constant at 1.25 MPa, and braking speeds are varied (30, 39, 49 and 59 m/s). Obtained data are displayed in Figure 24. Figure

**Table 24:** Composition (in % volume) and specimen designation [75]

| Ingredients | Variation of phenolic resin | | | Variation of fly ash | |
|---|---|---|---|---|---|
| | 20% PR* | 30% PR | 40% PR | 5% FA | 10% FA |
| NBR rubber, cashew dust, graphite, glass fiber, cast iron chip | 49 | 49 | 49 | 49 | 49 |
| Phenolic resin | 20 | 30 | 40 | 20 | 20 |
| Fly ash | 0 | 0 | 0 | 5 | 10 |
| Barite | 31 | 21 | 11 | 26 | 21 |

*The formulation of 20% PR also used for variation of fly ash amount with 0% volume of fly ash.

**Table 25:** Composition (in % volume) and specimen designations [76]

| Ingredients | Variation of cast iron chip | | | Variation of Cu short wire | |
|---|---|---|---|---|---|
| | WM | 2% CI | 4% CI | 2% Cu | 4% Cu |
| NBR rubber, cashew dust, glass fiber, phenolic resin | 57 | 57 | 57 | 57 | 57 |
| Graphite | 30 | 30 | 30 | 30 | 30 |
| Cast iron chip | 0 | 2 | 4 | 0 | 0 |
| Cu short wire | 0 | 0 | 0 | 2 | 4 |
| Barite | 13 | 11 | 9 | 11 | 9 |

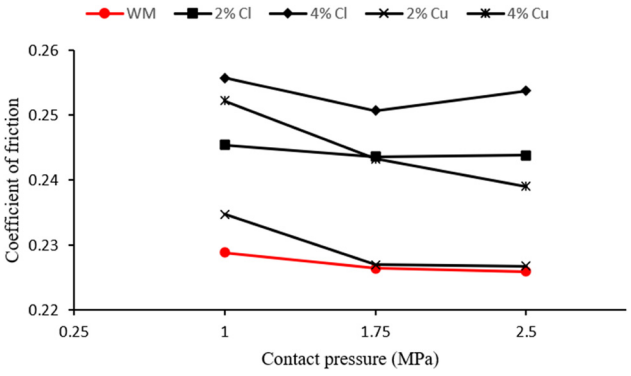


**Figure 22:** Coefficient of friction toward variation of contact pressure with sliding speed 5 m/s [76].

24 is drawn based on information and the study by Li and Yan [77].

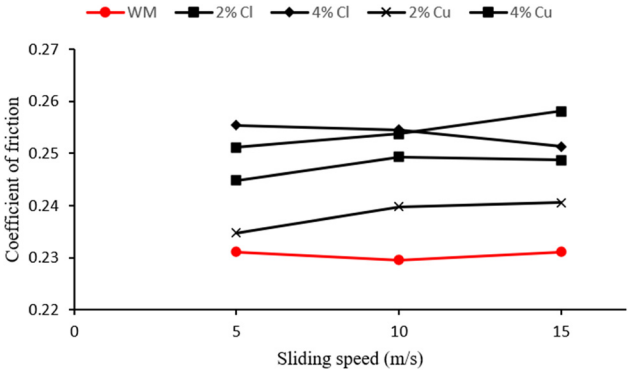


**Figure 23:** Coefficient of friction toward variation of contact pressure with contact pressure 1 MPa [76].

From the data displayed in Figure 24, block brake C/C and metallic have a coefficient that tends to be constant, while the C/C-SIC brake block forms a parabolic pattern, as the increase in the coefficient speed actually decreases and then increases slightly at the highest speed. The rate of wear of the C-C brake block has decreased along with the increase in speed. In contrast to the behavior exhibited by C-C brake blocks, metallic brake blocks demonstrate an increased wear rate at higher speeds. As for the C/C-SIC brake block, the pattern is inversely proportional to the results of the coefficient of friction [77].

Ertan [78] analyzed a combination of additional organic materials (cashew dust) and ceramics ($ZrSiO_4$ and $Fe_2O_3$) on brake block composites to achieve optimal performance. There are several variations of the composition used in this study displayed in Table 26.

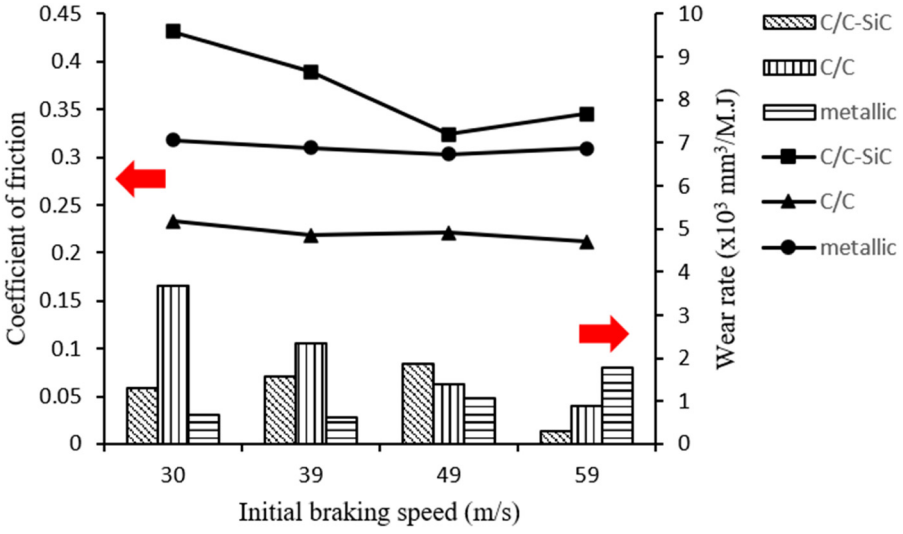


**Figure 24:** Coefficient of friction and wear rate of different materials [77].

**Table 26:** Ingredients of the friction materials investigated in this work (wt%) [78]

| Ingredients | | A1 | A2 | A3 | A12 | A13 | A23 | A123 |
|---|---|---|---|---|---|---|---|---|
| Ceramic-based abrasives | $ZrSiO_4$ | 10 | 3 | 3 | 6.5 | 6.5 | 3 | 6 |
| | $Fe_2O_3$ | 2 | 9 | 2 | 5.5 | 2 | 5.5 | 4 |
| Organic friction modifiers | Cashew dust | 3 | 3 | 10 | 3 | 6.5 | 6.5 | 5 |
| Reinforcements | | 25 | 25 | 25 | 25 | 25 | 25 | 25 |
| Binders | | 10 | 10 | 10 | 10 | 10 | 10 | 10 |
| Lubricants | | 20 | 20 | 20 | 20 | 20 | 20 | 20 |
| Fillers | | 30 | 30 | 30 | 30 | 30 | 30 | 30 |
| Density (g/cm$^3$) | | 2.13 | 2.11 | 1.80 | 2.03 | 2.01 | 1.95 | 2.05 |

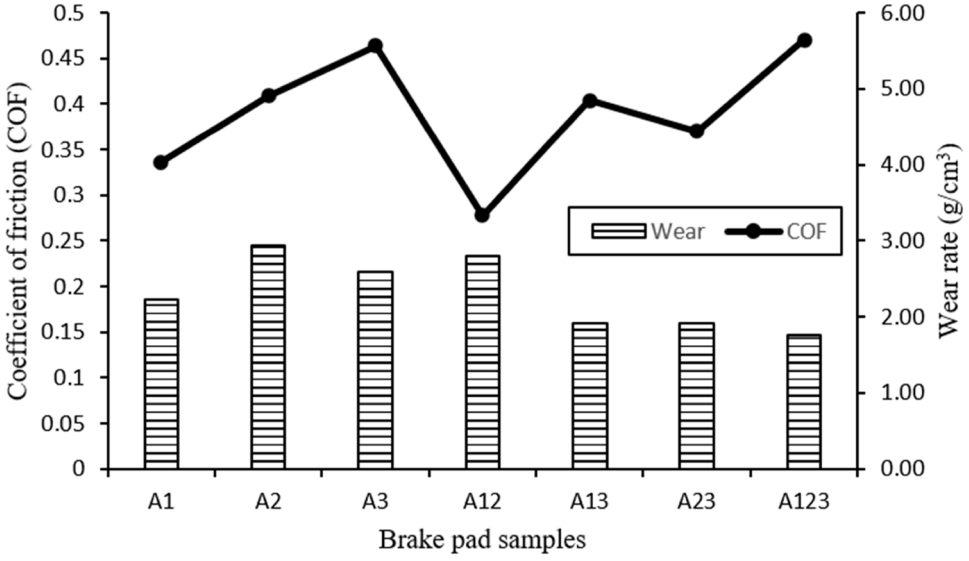


**Figure 25:** Friction test result for brake pad material [78].

Each sample was made to test friction and also the specific wear rate at a speed of 411 rpm with an emphasis force of 540 N. Obtained results are displayed in Figure 25. Figure 25 is drawn based on information and the study by Ertan [78]. The data obtained show that a combination of the proportion of the right organic matter and ceramics that provide optimal performance. Optimal performance is indicated by the coefficient of friction during stable testing and good wear resistance. A123 sample is an optimal combination in this study [78].

Maulana *et al.* [79] examined the characteristics of friction from brake material that uses cantala fiber as a reinforcement of brake block composites. The percentage of volume used in this study is displayed in Table 27.

Each sample was tested for the coefficient of friction using the pin-on-disc method. Some test variations are carried out with disc rotting speeds (3, 6, 9, 12 m/s) and contact pressure (0.25; 0.5; 0.75; 1 MPa). The results of the friction coefficient test are shown in Figures 26 and 27, while Figure 28 shows the specific wear results. Figures 26–28 are drawn based on information and the study by Maulana *et al.* [79]. The addition of cantala fiber to various braking conditions can decrease the coefficient of friction. Cantala fiber can increase wear resistance and stabilize the coefficient of brake material friction [79].

Choosri *et al.* [80] examined the potential for the use of coal ash and sugarcane ash as abrasive material in the composite brake block with the phenolic resin matrix. The composition used in this study is displayed in Table 28.

Each sample was testing the coefficient of friction using the pin-on-disc method with an emphasis force of 1 N Disc rotating speed of 33.7 cm/s and the length of the track as far as 1 km. The results of the test of the friction coefficient and also the specific wear rate are shown in Figures 29 and 30. Figures 29 and 30 are drawn based on information and the study by Choosri *et al.* [80]. The

**Table 27:** Volume fraction variations for Cantala fiber and $CaCO_3$ [79]

| Materials | Specimen code (v%) | | | |
|---|---|---|---|---|
| | CF0 | CF4 | CF8 | CF12 |
| Cantala fiber | 0 | 4 | 8 | 12 |
| $CaCO_3$ | 32 | 28 | 24 | 20 |

optimal composition is obtained in variations with the addition of secondary abrasives as much as 4%. The increasing composition of secondary abrasives actually increases the specific wear rate [80].

Ghosh *et al.* [81] examined the effect of the addition of Calcined Petroleum Coke (CPC) on the phenolic resin elastomer composite. The formula used in this study is displayed in Table 29.

Each sample was observed and tested the coefficient of friction and its wear rate at a rotary speed of 150 rpm for 30 min with contact pressure of 50 N. The test results were displayed in Figures 31 and 32. Figures 31 and 32 are drawn based on information and the study by Ghosh *et al.* [81]. The addition of CPC increased the resistance [81].

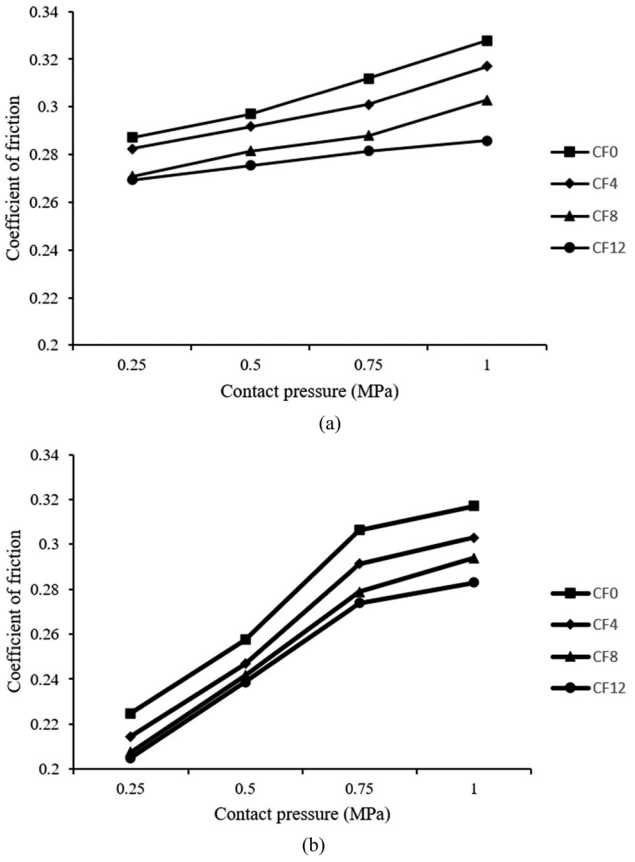


**Figure 26:** Effect of contact pressure and cantala fiber on coefficient of friction at a sliding speed of (a) 3 m/s and (b) 12 m/s [79].

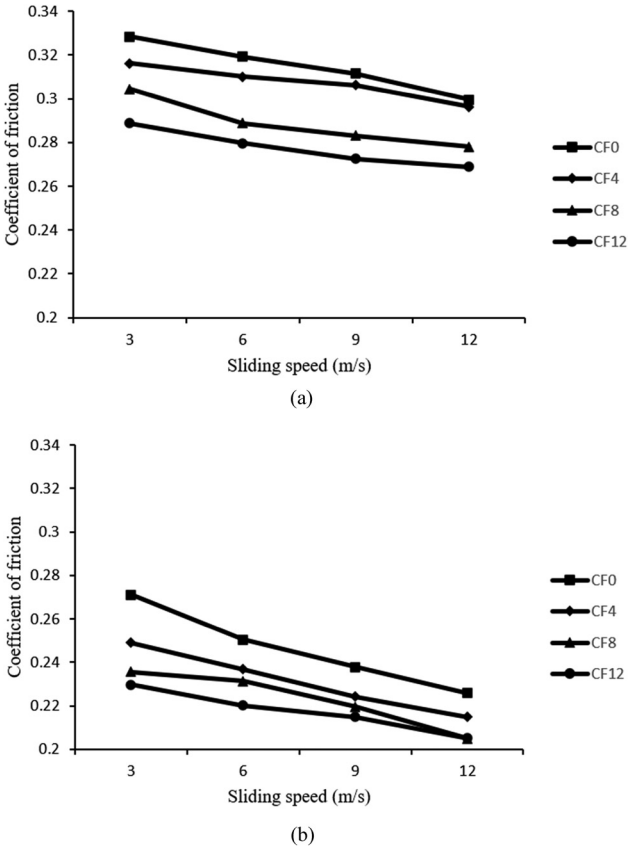


**Figure 27:** Effect of contact pressure and cantala fiber on coefficient of friction at a contact pressure of (a) 1 MPa and (b) 0.25 MPa [79].

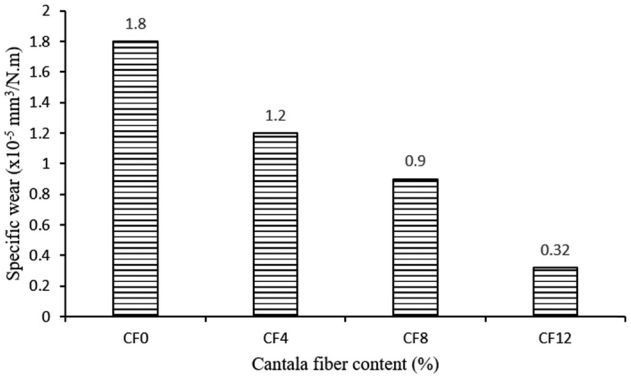


**Figure 28:** Effect of cantala fiber on specific wear [79].

**Table 28:** The ingredients for phenolic-based composite samples [80]

| Ingredients | Content (wt%) |
|---|---|
| Phenolic resin | 50 |
| S-Glass fiber | 15 |
| Silicon carbide | 8 |
| Graphite | 3 |
| Barium sulfate | 12 |
| Primary abrasives[a]/secondary abrasives[b] | 12/0, 8/4, 4/8, 0/12 |

[a]Alumina and silica.
[b]Fly ash and bagasse ash.

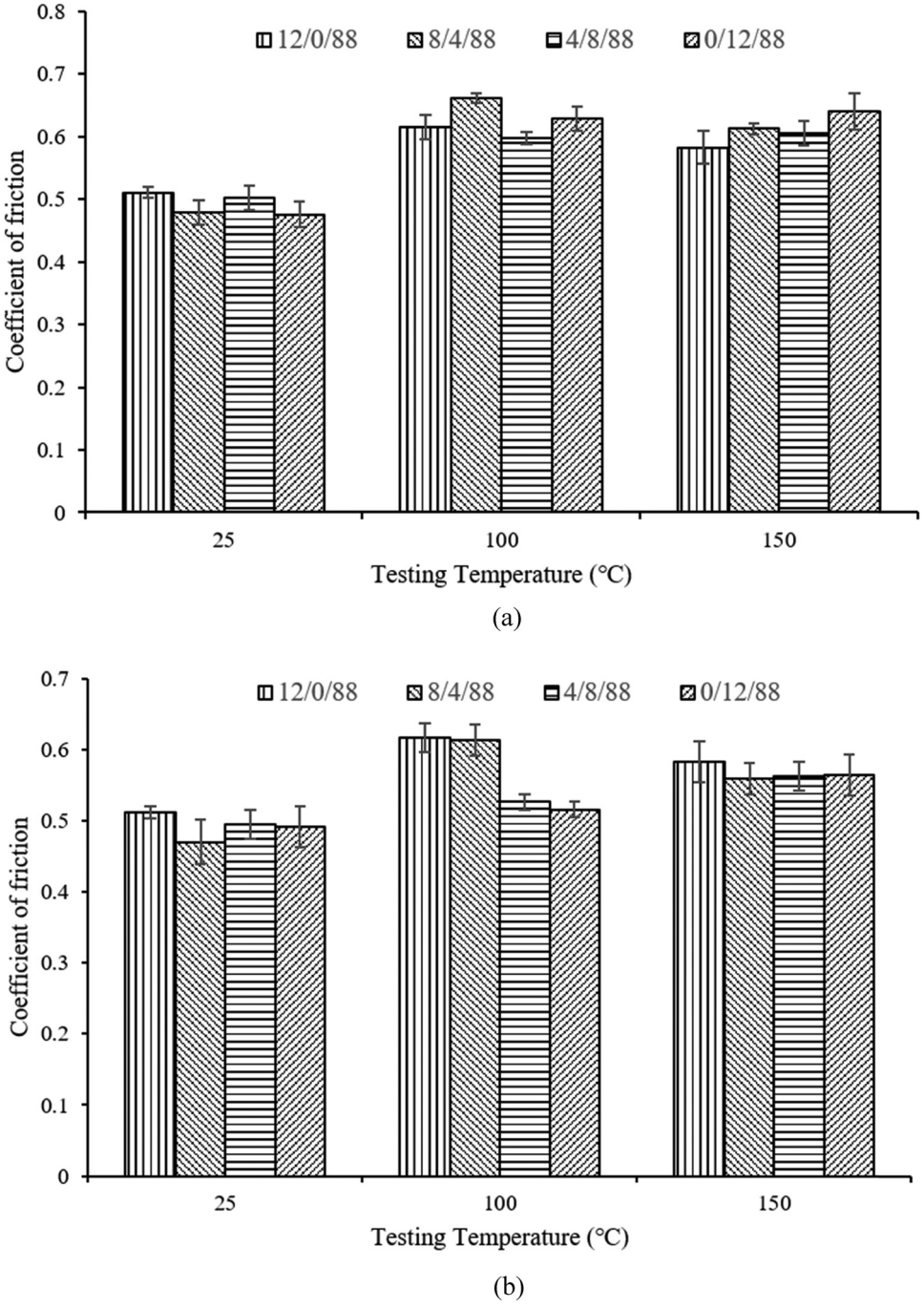


**Figure 29:** Coefficient of friction during pin on disk test for the phenolic based composite containing secondary abrasives: (a) fly ash and (b) bagasse ash [80].

Palmiyanto *et al.* [82] observed the potential that exists from the use of glass powder waste. Glass powder is used as a brake block constituent material because it has a high silica content that can improve the abrasive properties of brake blocks. Besides that, the use of this glass powder waste is able to save the environment because it is known that glass powder is a material that is difficult to decompose. The formula used in this study is shown in Table 30.

Each sample was then carried out the coefficient of friction and specific wear rate using tribometer pin on disk. The test parameters are varied into contact pressure (0.25, 0.5, 0.75, and 1 MPa) and disk rotary speed (2, 6, 9, 12 m/s). The results obtained are shown in Figures 33–35.

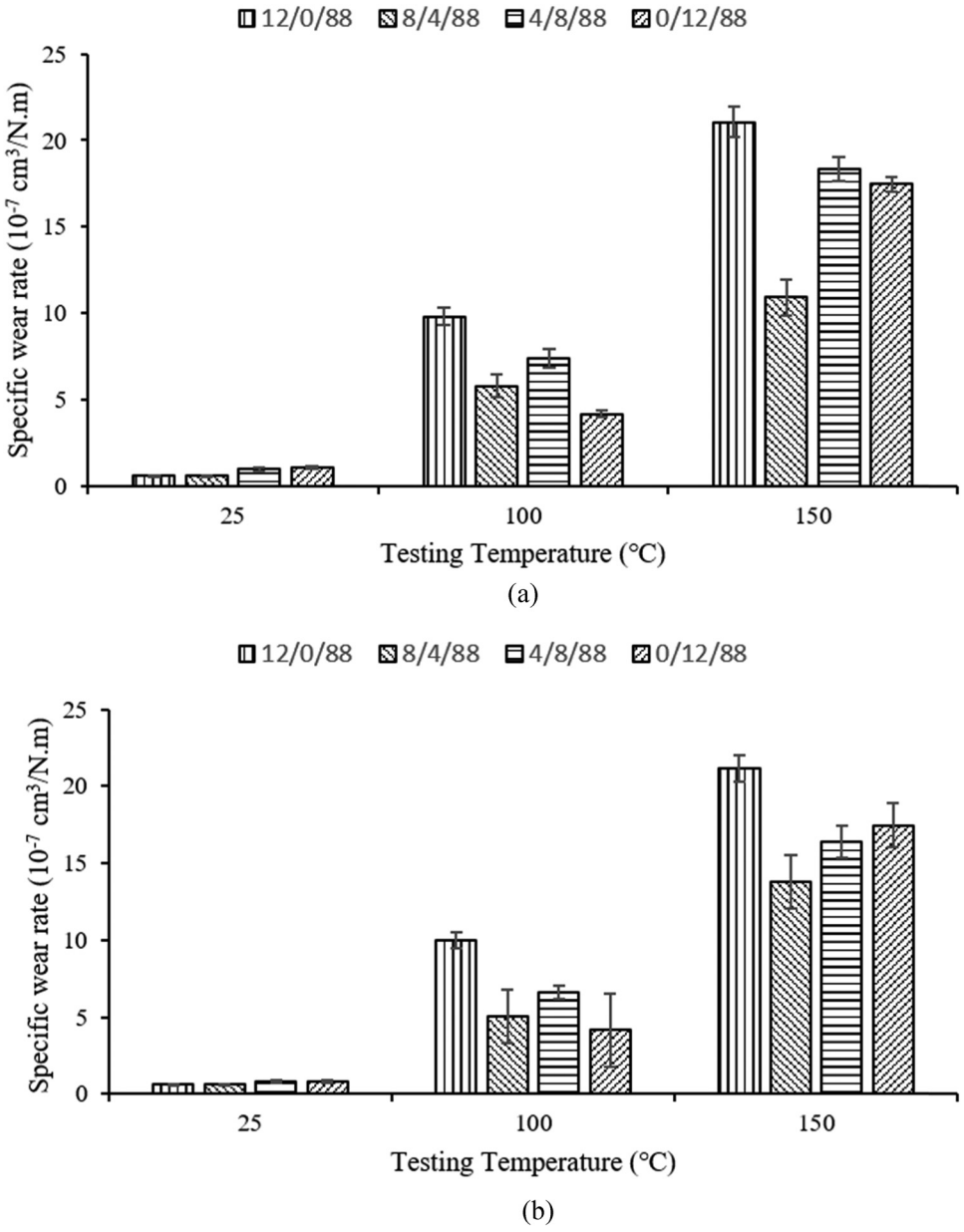


**Figure 30:** Specific wear rate during pin on disk test for the phenolic based composite containing secondary abrasives: (a) fly ash and (b) bagasse ash [80].

Figures 33–35 are drawn based on information and the study by Palmiyanto *et al.* [82]. The addition of glass powder can reduce the specific wear rate and increase the coefficient of friction [82].

Monreal *et al.* [83] observe the chances of the use of Latxa Sheep Wool as an organic fiber substitute that is often used in the manufacture of brake block composites. Organic fibers that are often used include aramid fiber, cellulose fiber, and polyacrylonitrile fiber. The composition used in this research is displayed in Table 31.

Each sample was tested for friction by varying the rotary speed (40, 60, 80, 90 km/h) and the pressure force (8, 14, 20, 26, 32 kN). The addition of Latxa Sheep Wool does not cause significant differences in the nature of wear (Table 32) [83].

Yanar *et al.* [84] examined the addition of hexagonal boron nitride (h-BN) on the characteristics of friction and wear of composite brake material. The nature of h-BN lubrication is good when compared to other materials with resistance at high temperatures.

**Table 29:** Formulation of the composites [81]

| Ingredients | Compositions | | | | | | | | | |
|---|---|---|---|---|---|---|---|---|---|---|
| | B | | C0.5 | | C1 | | C2 | | C3 | |
| | phr | Vol. (%) | phr | Vol. (%) | phr | Vol. (%) | phr | Vol. (%) | phr | Vol. (%) |
| PF resin | 100 | 43.8 | 100 | 38.9 | 100 | 34.9 | 100 | 29.1 | 100 | 24.8 |
| Hexamine | 10 | 3.9 | 10 | 3.5 | 10 | 3.1 | 10 | 2.6 | 10 | 2.3 |
| NBR + ZnO + St. acid + S + CBS + TQ | 79 | 40.6 | 79 | 35.9 | 79 | 32.4 | 79 | 26.8 | 79 | 22.9 |
| SRF black | 40 | 11.7 | 40 | 10.4 | 40 | 9.3 | 40 | 7.7 | 40 | 6.6 |
| CPC | 0 | 0 | 50 | 11.3 | 100 | 20.3 | 200 | 33.8 | 300 | 43.4 |

The composition used in this study is displayed in Table 33.

The results of testing the friction coefficient and wear rate of each sample (Table 33) are presented in Figure 36. Figure 36 is drawn based on information and the study by Yanar *et al.* [84]. From these results, it was found that the effect of adding h-BN optimal addition was obtained on the BN-2 sample by producing a good coefficient of friction, but the value of the rate of wear rate remains low [84].

Sunardi *et al.* [85] developed the brake lining with the addition of eggshell powder as a reinforcing material on the brake block composite. In this study, there are several variations in the addition of eggshell powder, with the treatment of calcinations that are varied shown in Table 34.

Each sample obtained by the coefficient of friction and specific wear rates using the tribometer pin on disk tester with a contact pressure of 0.75 MPa at a speed rate of 12 m/s disk shown in Figure 37. Figure 37 is drawn based on information and the study by Sunardi *et al.* [85]. From the tests that have been done, the conclusion of the brake lining with eggshell powder is calcined at 900°C for 120 min with a size of 200 mesh and the 25% fraction volume shows the best performance. This brake lining has a coefficient of friction and the optimal level of wear [85]. Table 35 illustrates milestone the use of advanced material for the development of braking design/train driving system.

# 6 Material manufacturing for braking design/train driving system

In a study of the failure analysis of railway brake blocks, Ajayi and Adeleke [86] used brake block specimens manufactured by the sand-casting method. The manufacturing process entails subjecting the material to melting in a reverberatory furnace for a duration of 1 h, subsequently followed by the pouring of the molten metal into a mold.

Laden *et al.* [87] created brake disc composite using the vortex method. The vortex method is chosen because it is economical and is also able to control various parameters such as concentration, size, shape, and type of reinforcement. The process involves a combination of aluminum alloys at a temperature that is 5°C below the liquidus temperature. Subsequently, the reinforcement is introduced to the molten metal, which has been stirred at a speed of 250 rpm. The next process is increased by the temperature to 750°C. Subsequently, the molten metal is poured into the mold (Figure 38). Figure 38 is drawn based on information and reference [87].

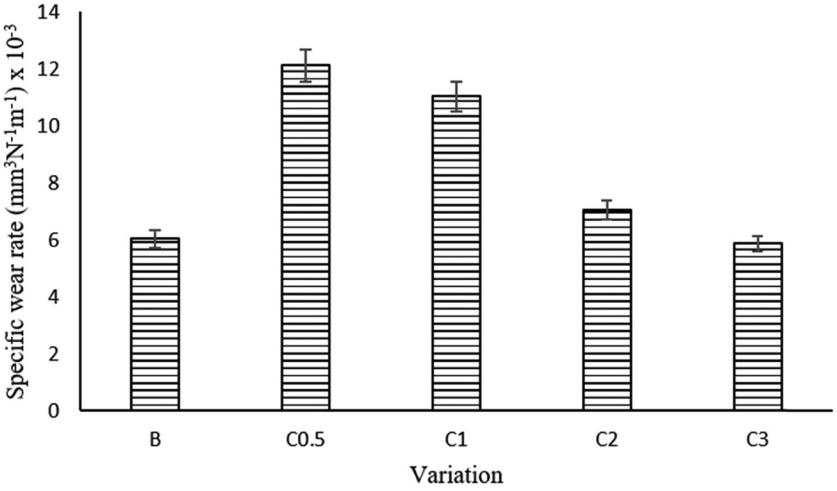


**Figure 31:** Specific wear rate as a function of sliding time for base composite (B) and CPC loaded composites [81].

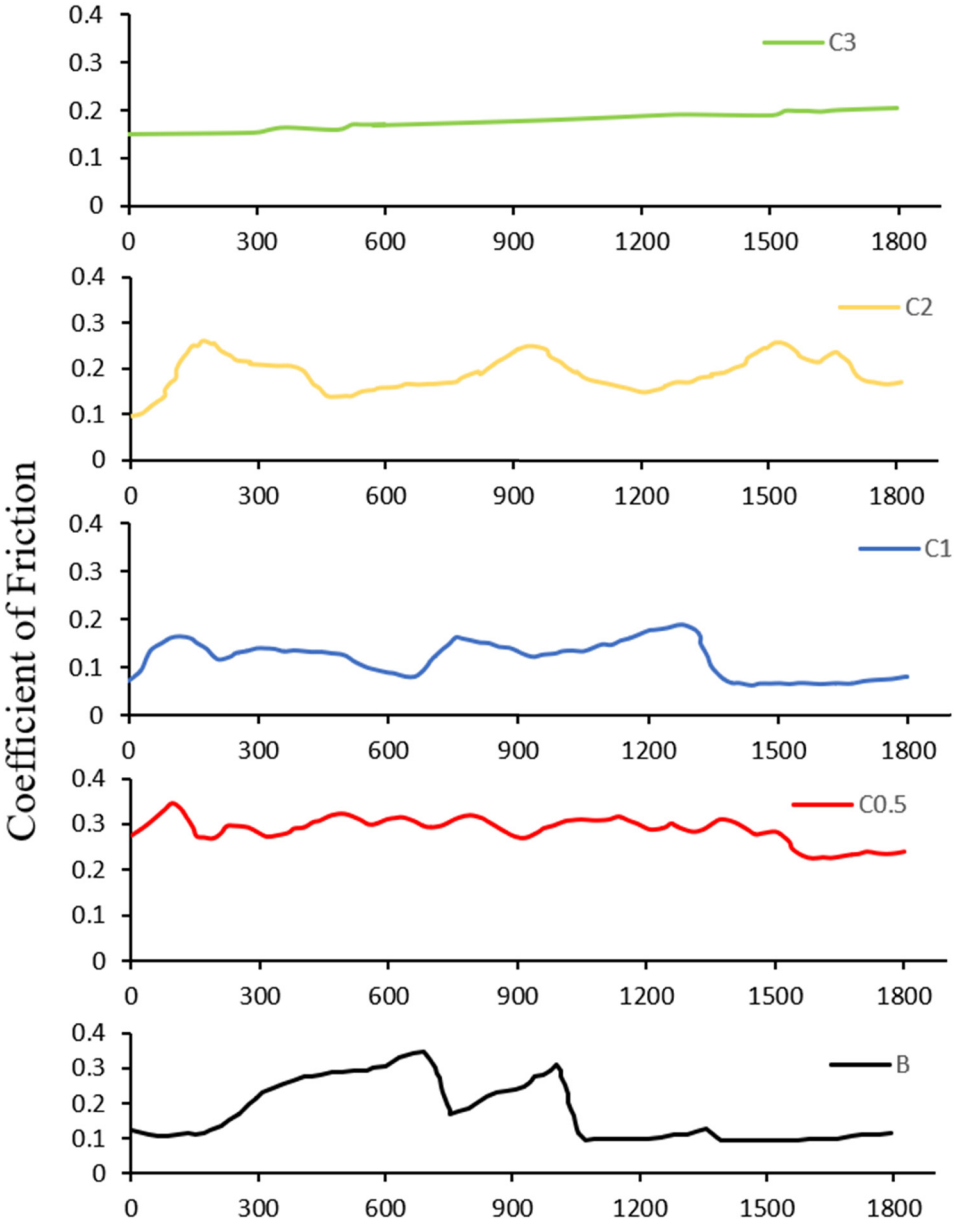


**Figure 32:** Coefficient of friction for (B) base composite and add CPC [81].

**Table 30:** The volume fraction of the specimen composition [82]

| Element | Glass powder composition (%) | | |
|---|---|---|---|
| | Non GP | GP 2 | GP 4 |
| Basic materials | 67 | 67 | 67 |
| $CaCO_3$ | 33 | 31 | 29 |
| Glass powder | 0 | 2 | 4 |

Abbasi *et al.* [88] conducted research related to brake block composites with polymer bases. The material is mixed using a banbury mixer by a compression process at a pressure of 6,000 psi at 145°C. After that the sample was carried out the postcuring process at 180°C for 12 h.

Ertan and Yavuz [71] observed the optimization of the brake block – making material with the manufacturing process with mixing, hot pressing, and sinter. All materials are mixed for 10 min with a speed of 3,000 rpm using a high-speed small-scale blender. Then the hot press process is carried out at 150°C with a pressure of 7.5 MPa for 5 min. During the hot press process, a gas release process is carried out to increase the cross-link reaction. Then the sinter process is carried out with an oven at 165°C for 12 h.

Arjmand and Shojaei [72] in their research in making brake blocks, the process of mixing was carried out by the

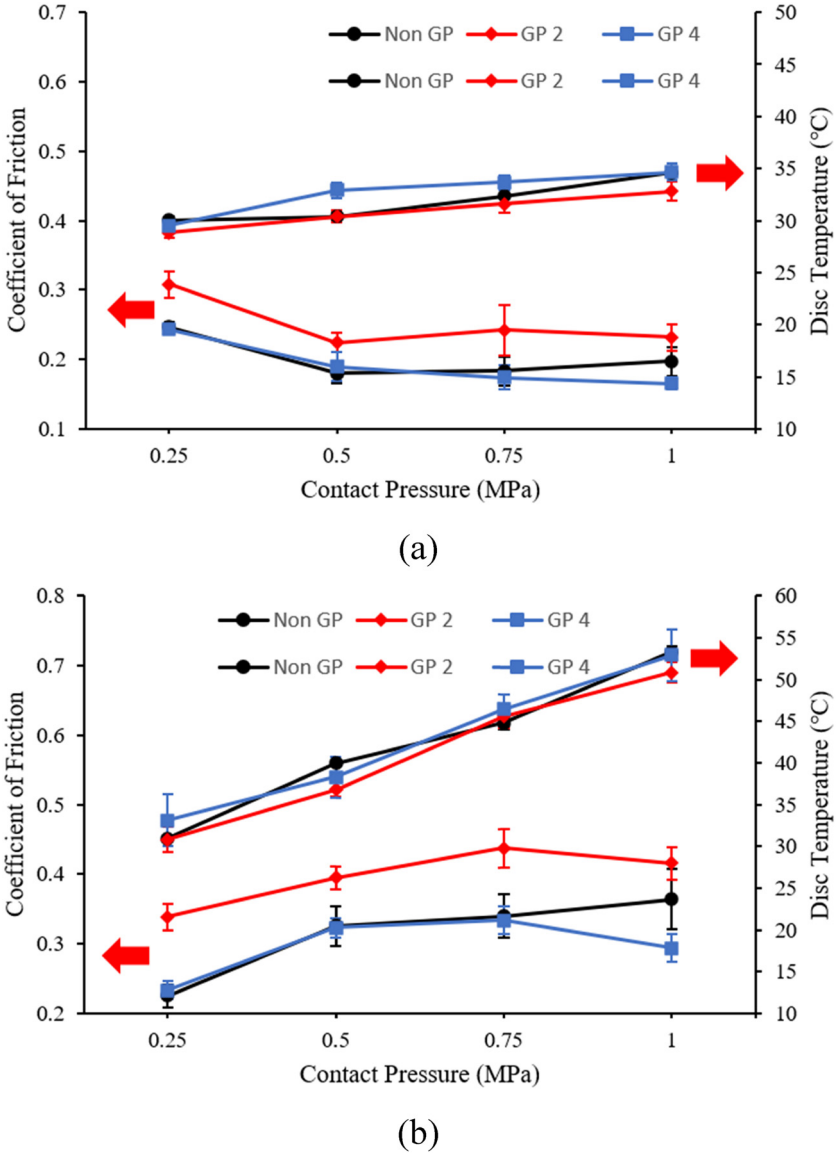


**Figure 33:** The coefficient of friction and disc temperature at various pressure with (a) low sliding speed (3 m/s) and (b) high sliding speed (12 m/s) [82].

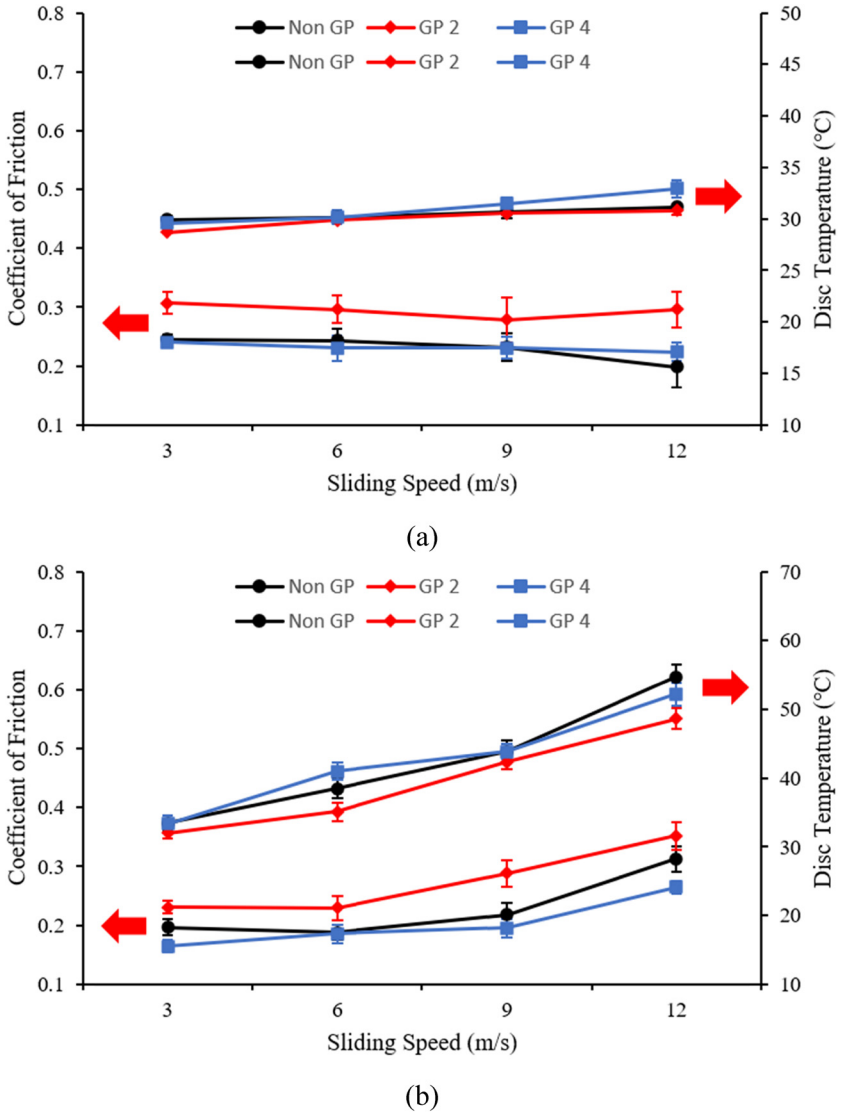


**Figure 34:** The coefficient of friction and disc temperature at various sliding speed with (a) low pressure (0.25 MPa) and (b) high pressure (1 MPa) [82].

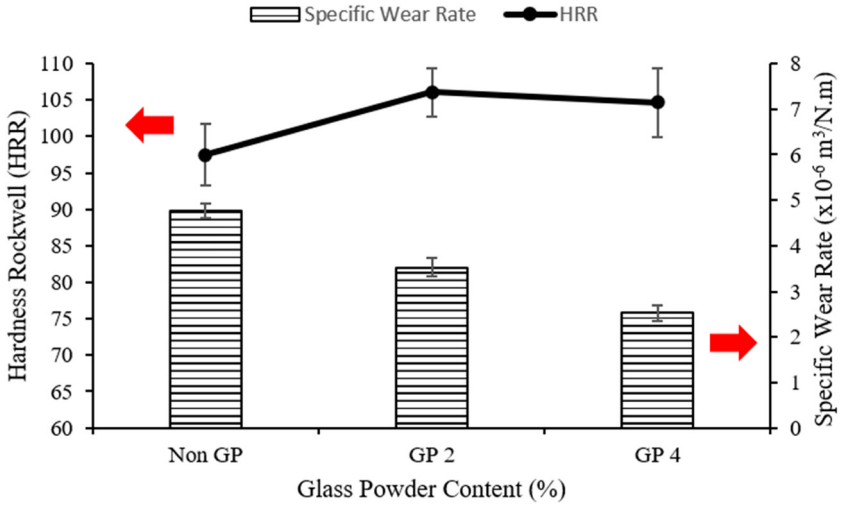


**Figure 35:** Hardness and specific wear rate at sliding speed 12 m/s and contact pressure 1 MPa [82].

**Table 31:** Compositions of the five friction materials studies (Vol) [83]

| Component | Control (%) | Aramid fiber (%) | Cellulose fiber (%) | PAN (%) | Sheep wool (%) |
|---|---|---|---|---|---|
| Friction material | 100 | 85 | 85 | 85 | 85 |
| Aramid fiber | — | 15 | — | — | — |
| Cellulose fiber | — | — | 15 | — | — |
| PAN fiber | — | — | — | 15 | — |
| Latxa sheep wool | — | — | — | — | 15 |

**Table 32:** Wear values for the five friction materials tested: mass loss and volume loss after the friction test [83]

| Material | Control | Aramid fiber | Cellulose fiber | PAN | Sheep wool |
|---|---|---|---|---|---|
| Mass loss (g) | 5.14 | 5.71 | 5.57 | 5.25 | 6.47 |
| Volume loss ($cm^3$) | 2.27 | 2.72 | 2.62 | 2.49 | 3.00 |

**Table 33:** Composition of the friction composite material (wt) [84]

| Ingredients | Sample codes/composition (wt%) | | | |
|---|---|---|---|---|
| | Base sample (BN-0) | 1.0 (BN-1) | 1.5 (BN-2) | 2.0 (BN-3) |
| Reinforcement (rockwool fiber, steel fiber and aramid fiber) | 38.0 | 38.0 | 38.0 | 38.0 |
| Binder (Phenolic resin) | 12.0 | 12.0 | 12.0 | 12.0 |
| Space filler (Barite) | 33.0 | 32.0 | 31.5 | 31.0 |
| Friction modifier (h-BN) | 0 | 1.0 | 1.5 | 2.0 |
| Others (Graphite, magnetite, CNSL) | 17.0 | 17.0 | 17.0 | 17.0 |

rubber and then by the resin, the mixing process was carried out for 20 min, then the hot press process was carried out at 145°C with a pressure of 100 MPa for 40 min by several Degassing processes. In the final stage, the postcuring process is carried out at 150°C for 5 h in the oven.

Shojaei *et al.* [73] also carried out the same process similar to that of by Arjmand and Shojaei by mixing for 20 min, and then a hot press process was carried out at 145°C with a pressure of 100 MPa for 40 min with several degassing processes. In the final stage, the postcuring process is carried out at 150°C for 5 h in the oven.

Wang *et al.* [89] developed modifications from phenolic resins. The manufacturing process begins with the powder mixing stage on the Z-Type Kneading Machine, and then the drying process was carried out. The mixed powder was carried out a hot press process at 155 ± 2°C

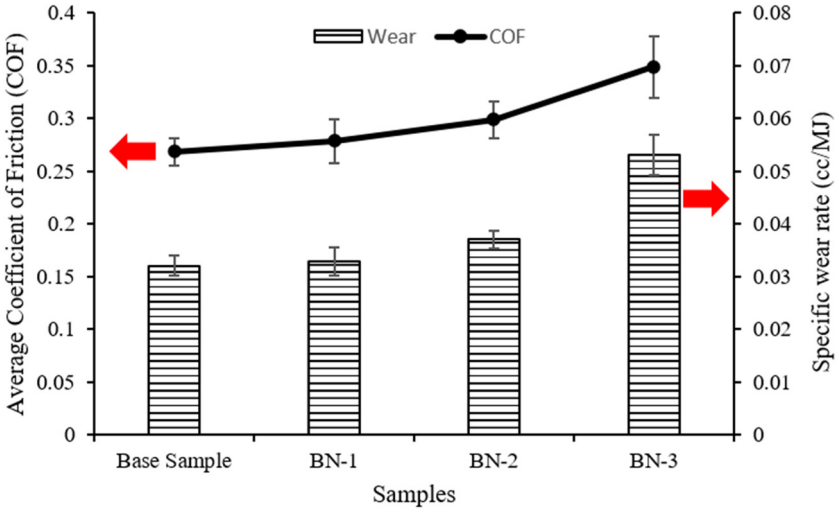


**Figure 36:** Variation of average CoF and specific wear rate with friction composite samples [84].

**Table 34:** Composition of the friction composite material (wt%) [85]

| Sample code | Composition | | | | | | | Calcination parameter | | |
|---|---|---|---|---|---|---|---|---|---|---|
| | Phenolic resin (%) | Bambo fiber (%) | Zinc powder (%) | Alumina powder (%) | Graphite powder (%) | Eggshell powder (%) | Bamboo powder (%) | Temperature (°C) | Time (min) | Particle size (mesh) |
| S1 | 35 | 10 | 5 | 10 | 10 | 5 | 25 | 100 | 60 | 80 |
| S2 | | | | | | 15 | 15 | 100 | 120 | 140 |
| S3 | | | | | | 25 | 5 | 100 | 180 | 200 |
| S4 | | | | | | 25 | 5 | 500 | 60 | 140 |
| S5 | | | | | | 5 | 25 | 500 | 120 | 80 |
| S6 | | | | | | 15 | 15 | 500 | 180 | 200 |
| S7 | | | | | | 15 | 15 | 900 | 60 | 80 |
| S8 | | | | | | 25 | 5 | 900 | 120 | 200 |
| S9 | | | | | | 5 | 25 | 900 | 180 | 140 |

with a pressure of 30 MPa for 50 min. This is continued with the postcured stage at 155 ± 2°C for 50 min.

Wang *et al.* [90] made hybrid fiber in the organic brake block on the passenger train through several stages. Phase 1 is the stage of mixing powder on the Z-Type Kneading Machine, and then the drying process is carried out. The mixed powder was carried out a hot press process at 155 ± 2°C with a pressure of 30 MPa for 50 min. This is continued with the postcured stage at 155°C for 50 min.

Baklouti *et al.* [91] made the brake block with the mixing process first, and then the cold preforming process wass carried out followed by hot molding at a temperature of 150°C for 18 min. The last process is the postcuring process at a temperature of 160°C for 10 h.

In their observation of three types of brake blocks, Surojo *et al.* [92] found that one was manufactured through a powder process that included mixing with a high-speed blender for 5 min. After that the fiber is added and continued the mixing process for 10 min. The next step is a cold press process with a pressure of 10 MPa then followed by a hot press at a pressure of 10 MPa with a temperature of 165°C for 60 min.

Peng *et al.* [93] focused on the ratio of Cu and Fe powder, which was manufactured by the initial process of mixing all powder (except graphite) on the V-Type Blender for 1.5 h. After that the graphite powder is inserted and then mixed for 30 min. The completion of the mixing process followed by the press process at a pressure of 300 MPa in a steel mold. The last process is carried out in the sinter process at a temperature of 980°C.

Sugözü [94] conducted research related to the use of fly ash in making brake blocks using the dry mixing,

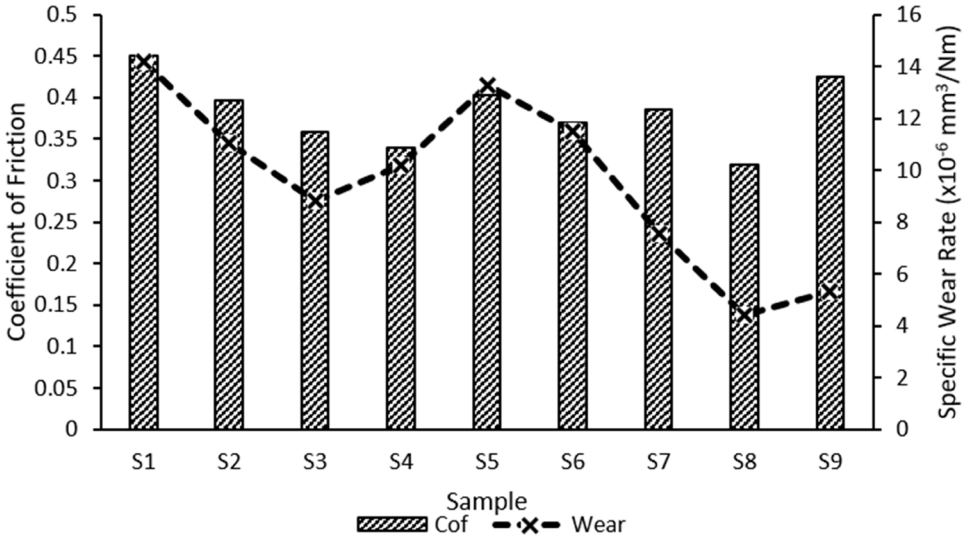


**Figure 37:** The values of the friction coefficient and specific wear rate [85].

**Table 35:** Milestone the use of advanced material for the development of braking design/train driving system

| Milestone | Author | Title | Important remarks | Ref. |
|---|---|---|---|---|
| 1987 | Mercer, C. I. | Medium Friction Non-Metallic Composition Brake Shoes as Direct Replacement for Cast Iron Brake Shoes on Rolling Stock | Better braking has been obtained by this middle-class brake lining compared to cast iron brake lining | [16] |
| 2003 | Sun-Zen Chen, Jiin-Huey Chern Lin and Chien-Ping Ju | Effect of Aluminum Content on Tribological Behavior of a Cu–Fe–C Based Friction Material Sliding against FC30 Cast Iron | The addition of aluminum to the optimal Cu-Fe-C material at 10% VT This is shown from the results of high and stable friction coefficient testing and high wear resistance | [67] |
| 2003 | Sun-Zen Chen, Jiin-Huey Chern Lin and Chien-Ping Ju | Effect of Graphite Content on the Tribological Behavior of a Cu–Fe–C Based Friction Material Sliding against FC30 Cast Iron | The addition of graphite will reduce the density of a material thereby reducing the wear resistance. The phenomenon that occurs in testing the coefficient of friction variations of C0 and C10 similar, decreases after a few minutes. The C20 variation is stable and high | [68] |
| 2003 | A.R. Ghaderi, M. Nili Ahmadabadi, H.M. Ghasemi | Effect of Graphite Morphologies on the Tribological Behavior of Austempered Cast Iron | Graphite morphology and austempering treatment affect the nature of cast iron tribology. Austempered cast iron compact with a denser graphite morphology shows the best wear resistance and lower friction coefficient | [69] |
| 2007 | K. Hirasata, K. Hayashi, Y. Inamoto | Friction and Wear of Several Kinds of Cast Irons Under Severe Sliding Conditions | The friction and wear of cast iron wear in severe friction conditions is influenced by its thermal and mechanical properties. By understanding the relationship between these parameters, the selection of cast iron that is suitable for heavy friction applications can be done more optimally | [70] |
| 2010 | Rukiye Ertan and Nurettin Yavuz | Optimisation of Brake Friction Material on Tribological Characteristics and Cost using Constrained Mixture Design Method | The composition of brake constituent materials is obtained by optimizing the proportion of reinforcement, lubricant, and abrasive materials | [71] |
| 2011 | M. Arjmand, A. Shojaei | Tribological Characteristics of RBFMS | Fiber plays an important role in the Tribological nature of RBFMS. Steel wool and aramid pulp have different effects on CoF, friction recovery, wear rates, and overall performance. The selection of fiber and concentration needs to be adjusted to certain applications and friction requirements | [72] |
| 2011 | Akbar Shojaei, Mohammad Arjmand, Amir Saffar | Studies on the Friction and Wear Characteristics of RBFMS Containing Carbon and Cellulose Fibers | Carbon fiber increases wear resistance and RBFMS friction stability without affecting too much CoF. Cellulose fiber increases CoF but has a negative impact on worn endurance | [73] |
| 2013 | Gongjun Cui, Qinling Bi, Shengyu Zhu, Licai Fu, JunYang, Zhuhui Qiao, Weimin Liu | Synergistic Effect of Alumina and Graphite on Bronze Matrix Composites: Tribological Behaviors in Sea Water | The addition of alumina and nickel coated graphite in bronze composites can increase wear resistance and improve friction performance | [74] |
| 2014 | E. Surojo, Jamasri, V. Malau, M. N. Ilman | Effects of Phenolic Resin and Fly Ash on Coefficient of Friction of Brake Shoe Composite | The composition of phenolic resins and fly ash affects the compound brake compound friction coefficient. Control ratio of both materials can be done to regulate the coefficient of friction according to braking needs | [75] |
| 2015 | E. Surojo, Jamasri, V. Malau, M. N. Ilman | Investigation of Friction Behaviors of Brake Shoe Materials using Metallic Filler | Cast iron chip and Cu short wire affect the increase in the coefficient of friction of brake shoe material | [76] |

(*Continued*)

**Table 35:** *Continued*

| Milestone | Author | Title | Important remarks | Ref. |
|---|---|---|---|---|
| 2015 | Gen Li, Qingzhi Yan | Comparison of Friction and Wear Behavior Between C/C, C/C-SiC and Metallic Composite Materials | Metal brake pads have the lowest wear rate at low speed, the highest at high speed. Brake pads C/C-SIC has the best wear resistance at high speed | [77] |
| 2016 | Rukiye Ertan | Synergistic Effect of Organic and Ceramic Based Ingredients on The Tribological Characteristics of Brake Friction Materials | The ideal composition of brake friction materials by combining organic and ceramic materials in the right proportion. This combination produces a stable friction coefficient and good wear resistance, making it suitable for brake applications that require high performance and reliability | [78] |
| 2018 | Ilham Taufik Maulana, Eko Surojo, Nurul Muhayat, Wijang Wisnu Raharjo | Frictional Characteristics of Friction Brake Material Using Cantala Fibers as Reinforcement | Cantala fiber is effective in improving the performance and durability of friction brake material | [79] |
| 2018 | Saowapa Choosri, Narongrit Sombatsompop, Ekachai Wimolmala, Sirinthorn Thongsang | Potential Use of Fly Ash and Bagasse Ash as Secondary Abrasives in Phenolic Composites for Eco-Friendly Brake Pads Applications | Coal ash and sugarcane ash have the potential to be used as a substitute for the main abrasive mineral in phenolic -based brake lining, so it is more environmentally friendly | [80] |
| 2020 | Prosenjit Ghosh, Shib Shankar Banerjee, Dipak Khastgir | Elastomer Modified Phenolic Resin-Based Composites with Reduced Scale Friction: Influence of Calcined Petroleum Coke on Tribological and Thermo-Mechanical Behavior | The addition of calcined petroleum coke (CPC) has the potential to increase wear resistance and thermal performance of brake composites without significantly reducing the coefficient of friction | [81] |
| 2021 | M.H. Palmiyanto, E. Surojo, D. Ariawan, F. Imaduddin | Waste Glass Powder as a Sustainable Abrasive Material for Composite Brake Block | Glass powder has the potential to be used as abrasive material on composite brake blocks | [82] |
| 2021 | Pablo Monreal, Javier Oroz, Kike Gutierrez, Isabel Claveria Ambroj | Natural Latxa Sheep Wool as an Environmentally Friendly Substitute for Specific Organic Fibers in Railway Friction Materials: A Preliminary Approach | Latxa Sheep Wool has the potential as a substitute for organic fiber in the railroad brake block | [83] |
| 2022 | Harun Yanar, Gencaga Purcek, Muhammed Demirtas, Hasan Huseyin Ayar | Effect Of h-BN Addition on Friction Behavior of Low-Steel Composite Brake Pad Material for Railway Applications | The addition of h-BN in a certain amount can increase the stability of friction and reduce the wear of composite brake material | [84] |
| 2023 | Sunardi, Dody Ariawan, Eko Surojo, Aditya Rio Prabowo, Hammar Ilham Akbar, Agung Sudrajad, Harjo Seputro | Optimization of Eggshell Particles to Produce Ecofriendly Green Fillers with Bamboo Reinforcement in Organic Friction Materials | The addition of eggshells can increase the rate of wear, the hardness and the rate of wear increase with the addition of eggshells particles, whereas, if the high friction coefficient is needed, the bamboo composition in the fiber and the shape of the added particles must be more | [85] |

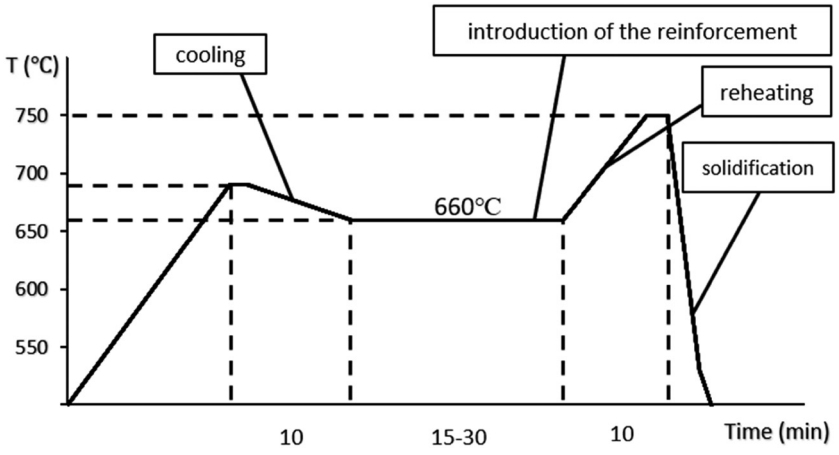


**Figure 38:** Typical production diagram of the Al-SiC composite brake disc [87].

**Table 36:** Manufacturing procedure for brake blocks [94]

| | Conditions | | |
|---|---|---|---|
| **Procedure** | **Time (min)** | **Pressure (MPa)** | **Temperature (°C)** |
| Mixing | 10 | — | Room temperature |
| Pre-forming | 2 | 8 | Room temperature |
| Hot-pressing | 10 | 10 | 150 |

preforming, and hot-pressing methods. The mixing process is done with a blender for 10 min. After that the preforming process was carried out with a pressure of 8 MPa for 2 min, then the hot press process is continued at a pressure of 10 MPa at 150°C for 10 min as shown in Table 36.

Zhang *et al.* [95] observed the addition of Ni-coated graphite to the brake lining with the main material of copper. The process of manufacturing brake pad used by the powder metallurgy method. First, all powder is mixed on the V-shaped mixer for 10 h. The second is a cold press process with a pressure of 400 MPa using Steel Die. The three sintering processes at a temperature of 950°C with a pressure of 3 MPa for 2 h.

Zhang *et al.* [96] observed the phenomenon that occurred in the brake lining with the main material of copper. The manufacturing process through the first few steps of the material is mixed on the V-shaped mixture for 8 h. Then a cold pressing process was carried out 400 MPa pressure for 2 min. Finally, the sintering process is carried out with a pressure of 3 MPa for 2 h at 950°C.

Palmiyanto *et al.* [82] see the potential possessed from glass powder waste as abrasive material. The manufacturing process in making brake blocks is carried out by mixing process, cold press process, hot press process, and postcuring. The process begins with mixing powder using a blender for 5 min and then inserted fibers followed by the mixing process for 3 min. The cold press process is carried out at a pressure of 40 MPa for 10 min. Then the hot press process is continued at a temperature of 150°C for 10 min at a pressure of 40 MPa. The final step is taken by the process of posting by heating from room temperature (30°C) at 140°C for 1 h and then from 140°C, the temperature is raised gradually to 180°C for 6 h, followed by the provision of 180°C to space temperature (30°C) for 30 min.

Research conducted by Wang *et al.* [97] examined related to tribology properties of brake disc material for a high-speed train. The manufacturing process uses a vacuum induction furnace. Each brake block goes through the normalized, hardened, and tempered process. The normalizing temperature used is 950°C, the quenching temperature is 920°C, and then the temperature is tempering at 600°C. Table 37 illustrates milestone material manufacturing for braking design/train driving system.

# 7 Conclusion

Explanation related to the development of the driving system on the railroad, especially in the braking system such as the development of braking system technology, failures that arise, financial losses, the use of advanced material, and the manufacturing process is discussed in this article. Some of the comments are summarized as follows:

- The development of technology in the railroad braking system starts from the fifteenth century to the present, and the development of both the railroad wheels, brake block/brake pad, and the testing methods used are continuously done.

**Table 37:** Milestone material manufacturing for braking design/train driving system

| Milestone | Author | Title | Important remarks | Ref. |
|---|---|---|---|---|
| 1997 | John Ade Ajayi and O. A. Adeleke | Failure Analysis of Railway Brake Blocks | Failure to production of local shoe brake blocks is caused by differences in microstructure composition | [86] |
| 2000 | K. Laden, J.D. Gu´erin, M. Watremez, J.P. Bricout | Frictional Characteristics of Al–SiC Composite Brake Discs | Al-SIC composites have the potential to be railroad brake material. Wear resistance, coefficient of friction and good operating temperature | [87] |
| 2001 | F. Abbasi, A. Shojaei, A. A. Katbab | Thermal Interaction between Polymer-Based Composite Friction Materials and Counterfaces | Optimization of modulus elasticity and thermal conductivity can improve brake block performance | [88] |
| 2010 | Rukiye Ertan, Nurettin Yavuz | Optimization of Brake Friction Material on Tribological Characteristics and Cost Using Constrained Mixture Design Method | Proportional raw materials for brake materials that have high friction performance and low production costs | [71] |
| 2011 | M. Arjmand, A. Shojaei | Tribological Characteristics of RBFMS | Fiber plays an important role in the tribological nature of RBFMS. Steel wool and aramid pulp have different effects on cof, friction recovery, wear rates, and overall performance. The selection of fiber and concentration needs to be adjusted to certain applications and friction requirements | [72] |
| 2011 | Akbar Shojaei, Mohammad Arjmand, Amir Saffar | Studies on the Friction and Wear Characteristics of RBFMS Containing Carbon and Cellulose Fibers | Carbon fiber increases wear resistance and RBFMS friction stability without affecting too much cof. Cellulose fiber increases cof but has a negative impact on worn endurance | [73] |
| 2011 | Haiqing Wang, Xingyang Wu, Xujun Liu, Peihong Cong | Application Study of a Modified Phenolic Resin as Binder for Hybrid Fibers Reinforced Brake Pad for Railroad Passenger-Coach Braking | Development of phenolic resin modification meets the existing requirements | [89] |
| 2011 | Haiqing Wang, Guangshan Zhuang, Chengguo Wang, Shuwei Zheng | Practical Application Study of Hybrid Fibers Reinforced Organic Brake Pad for Railroad Passenger-Coach Braking | Development brake blocks can meet the existing standard, longer life, safety and comfort | [90] |
| 2013 | Mouna Baklouti, Riadh Elleuch, Anne-Lise Cristol, Denis Najjar, Yannick Desplanques | Relationships Between the Heterogeneous Microstructure, the Mechanical Properties and the Braking Behavior of an Organic Brake Lining Material | Microstructure affects the performance of the brake block | [91] |
| 2017 | E. Surojo, Jamasri, V. Malau, M.N. Ilman | Characteristic Evaluation of Brake Block Material | The ratio of three types of brake blocks in this study shows that the composite brake block has a stable friction coefficient and a higher wear resistance than the cast brake block | [92] |
| 2018 | Tao Peng, Qingzhi Yan, Gen Li, Xiaolu Zhang | The Influence of Cu/Fe Ratio on the Tribological Behavior of Brake Friction Materials | The Cu/Fe ratio affects the nature of the tribology from the brake block | [93] |
| 2018 | Banu Sugözü | Tribological Properties of Brake Friction Materials Containing Fly Ash | Alternative fly ash as a filler for making brake blocks | [94] |
| 2019 | Peng Zhang, Lin Zhang, Kangxi Fu, Peifang Wu, Jingwu Cao, Cairang Shijia, Xuanhui Qu | Effects of Ni-Coated Graphite Flake on Braking Behavior of Cu-Based Brake Pads Applied in High-Speed Railway Trains | Graphite coating using nickel can increase the stability of performance and heat resistance to the brake lining | [95] |
| 2020 | Peng Zhang, Lin Zhang, Dongbin Wei, Peifang Wu, Jingwu Cao, Cairang Shijia, Xuanhui Qu | A High-Performance Copper-Based Brake Pad for High-Speed Railway Trains and its Surface Substance Evolution and Wear Mechanism at High Temperature | The development of brake lining with the main constituent of copper can increases the security and efficiency on high -speed railroad | [96] |
| 2021 | | | | [82] |

(*Continued*)

**Table 37:** *Continued*

| Milestone | Author | Title | Important remarks | Ref. |
|---|---|---|---|---|
| | M.H. Palmiyanto, E. Surojo, D. Ariawan, F. Imaduddin | Waste Glass Powder as a Sustainable Abrasive Material for Composite Brake Block | Glass powder waste has the opportunity as an abrasive as a substitute for pure silica | |
| 2022 | Jinnan Wang, Muhammad Qasim Zafar, Yunbo Chen, Peng Pan, Lingli Zuo, Haiyan Zhao, and Xiangjun Zhang | Tribological Properties of Brake Disc Material for a High-Speed Train and the Evolution of Debris | The stability of the braking system is very important for high-speed rail operational security | [97] |

- Failure is a common occurrence in railroad braking systems, manifesting in various forms such as flat braking, shelling, thermal cracking, and the formation of hot spots.
- Final losses are generally divided into fatal accidents, serious accidents, and deaths.
- The use of advanced material on rail brake blocks continues to be developed including the use of metal composites, synthetic composites, and natural fiber composites as a substitute for cast iron materials that have many shortcomings.
- The railroad brake block manufacturing process initially used the casting method and then developed using the powder metallurgical process. The metallurgical method of this powder continues to be developed, which affects the results of the railroad brake block.

From some of the things that have been summarized earlier, the development of the braking system on the train really needs to be developed. This will support the realization of rails as public transportation on land with an accident rate and low failure.

**Acknowledgments:** This research was supported by the Directorate of Research, Technology and Community Service, Directorate General of Higher Education, Research, and Technology, Ministry of Education, Culture, Research, and Technology, under scheme "*Penelitian Tesis Magister (PTM)*" with research grant number: 1280.1/UN27.22/PT.01.03/2023. We would also like to express our gratitude to our colleagues at Universitas Sebelas Maret for their valuable insights and expertise, which significantly contributed to the success of this research.

**Funding information:** The publication funding of this article was supported by Ministry of Education, Culture, Research, and Technology.

**Author contributions:** FI: writing – original draft, writing – review & editing, validation, formal analysis, visualization, investigation. ES: supervision, conceptualization, methodology, project administration, funding acquisition, validation. ARP: supervision, conceptualization, data curation, writing – review & editing, investigation. All authors have accepted responsibility for the entire content of this manuscript and approved its submission.

**Conflict of interest:** The authors state no conflict of interest.

**Data availability statement:** All data generated or analyzed during this study are included in this published article.

# References


[1] Ham YS, Hong JS, Oh TY, Paik YN. Development of a torsion-free brake shoe holder hanger for the bogie of railway freight car. Key Eng Mater. 2005;297–300:316–21.

[2] Yin J, Tang T, Yang L, Xun J, Huang Y, Gao Z. Research and development of automatic train operation for railway transportation systems: A survey. Transp Res Part C Emerg Technol. 2017;85:548–72. doi: 10.1016/j.trc.2017.09.009.

[3] Zuo J, Dong L, Ding J, Wang X, Diao P, Yu J. Design and validation of a self-powered device for wireless electronically controlled pneumatic brake and onboard monitoring in freight wagons. Energy Convers Manag. 2021;239:114229. doi: 10.1016/j.enconman.2021.114229.

[4] Günay M, Korkmaz ME, Özmen R. An investigation on braking systems used in railway vehicles. Eng Sci Technol Int J. 2020;23(2):421–31.

[5] Piechowiak T. Pneumatic train brake simulation method. Veh Syst Dyn. 2009;47(12):1473–92.

[6] Eckert JJ, Teodoro ÍP, Teixeira LH, Martins TS, Kurka PRG, Santos AA. A fast simulation approach to assess draft gear loads for heavy haul trains during braking. Mech Based Des Struct Mach. 2021;51(3):1606–25. doi: 10.1080/15397734.2021.1875233.

[7] Ogasa M. Application of energy storage technologies for electric railway vehicles-examples with hybrid electric railway vehicles. IEEJ Trans Electr Electron Eng. 2010;5(3):304–11.

[8] Fletcher RG. Regenerative equipment for railway rolling stock. Power Eng J. 1991;5(3):105–13.

[9] Al Zubaidi FN, Asaad LM, Alshalal I, Rasheed M. The impact of zirconia nanoparticles on the mechanical characteristics of 7075 aluminum alloy. J Mech Behav Mater. 2023;32(1):1–10.

[10] Alshalal I, Al-Zuhairi HMI, Abtan AA, Rasheed M, Asmail MK. Characterization of wear and fatigue behavior of aluminum piston alloy using alumina nanoparticles. J Mech Behav Mater. 2023;32(1):1–7.

[11] Bruni S, Vinolas J, Berg M, Polach O, Stichel S. Modelling of suspension components in a rail vehicle dynamics context. Veh Syst Dyn. 2011;49(7):1021–72.

[12] Djukić M, Rusov S, Mitrovic Z. A fuzzy model for an increase in locomotive traction force. Transport. 2010;25(1):36–45.

[13] Levchenkov A, Gorobetz M, Ribickis L, Balckars P. Immune algorithm for intelligent controller in braking system of electric railway transport. Proceedings of 14th International Power Electronics and Motion Control Conference EPE-PEMC 2010. 2010. p. 30–7.

[14] Dolbear KD, Watson JC. The development of friction pairs for intermediate to very high duty railway applications. Proc Inst Mech Eng Part F J Rail Rapid Transit. 1994;208(2):109–13.

[15] Roe MJ. Electric Bo-Bo-Bo locomotives for New Zealand Railways. Proc Inst Mech Eng Part D, Transp Eng. 1988;202(1):21–31.

[16] Mercer CI. Medium friction non-metallic composition brake shoes as direct replacement for cast iron brake shoes on rolling stock. Railw Eng. 1987;201(2):20–8.

[17] Wise S. Railway wheelsets – a critical review. Proc Inst Mech Eng, Part D: Transp Eng. 1987;201(4):257–71.

[18] Berndt PJ, Schweiger W. Experimental and theoretical investigation of brake squeal with disc brakes installed in rail vehicles. Wear. 1986;113(1):131–42.

[19] Wilkinson DT. Electric braking performance of multiple-unit trains. GEC Rev. 1985;1(1):37–43.

[20] Hasegawa I, Uchida S. Braking systems. Jpn Railw Transp Rev. 1999;7:168–82.

[21] Benseddiq N, Weichert D, Seidermann J, Minet M. Optimization of design of railway disc brake pads. Proc Inst Mech Eng Part F J Rail Rapid Transit. 1996;210(1):51–61.

[22] Desplanques Y, Degallaix G, Copin R, Berthier Y. A tribometer for the study of materials under railway braking conditions. Tribol Ser. 2001;39:381–91.

[23] Hecht M. European freight vehicle running gear: today's position and future demands. Proc Inst Mech Eng Part F J Rail Rapid Transit. 2001;215:1–11.

[24] Grosse M, Ceretti M, Ottlinger P. Distribution of radial strain in a disc-braked railway wheel measured by neutron diffraction. Appl Phys A Mater Sci Process. 2002;74:1400–2.

[25] Nankyo M, Ishihara T, Inooka H. Feedback control of brake system on railway vehicle considering non-linear property and dead time. IMECE. 2003. p. 1–6.

[26] Cartigny F, Dufrénoy P, Desmet B. A thermal analysis of a new railway brake concept using liquid cooling. Proc Inst Mech Eng Part F J Rail Rapid Transit. 2004;218(2):79–88.

[27] Handoko Y, Dhanasekar M. An inertial reference frame method for the simulation of the effect of longitudinal force to the dynamics of railway wheelsets. Nonlinear Dyn. 2006;45(3–4):399–425.

[28] Vernersson T. Temperatures at railway tread braking. Part 1: modelling. Proc Inst Mech Eng Part F J Rail Rapid Transit. 2007;221(2):167–82.

[29] Douglas H, Roberts C, Hillmansen S, Schmid F. An assessment of available measures to reduce traction energy use in railway networks. Energy Convers Manag. 2015;106:1149–65. doi: 10.1016/j.enconman.2015.10.053.

[30] Šamec B, Potrč I, Šraml M. Low cycle fatigue of nodular cast iron used for railway brake discs. Eng Fail Anal. 2011;18(6):1424–34.

[31] Vakkalagadda MRK, Srivastava DK, Mishra A, Racherla V. Performance analyses of brake blocks used by Indian Railways. Wear. 2015;328–329:64–76. doi: 10.1016/j.wear.2015.01.044.

[32] Sawczuk W, Ulbrich D, Kowalczyk J, Merkisz-Guranowska A. Evaluation of wear of disc brake friction linings and the variability of the friction coefficient on the basis of vibroacoustic signals. Sensors. 2021;21(17):1–21.

[33] Somà A, Aimar M, Zampieri N. Simulation of the thermal behavior of cast iron brake block during braking maneuvers. Appl Sci. 2021;11(11):1–12.

[34] Lu C, Jiang X, Chen X, Mo J. Experimental study on the evolution of friction and wear behaviours of railway friction block during temperature rise under extreme braking conditions. Eng Fail Anal. 2022;141:106621. doi: 10.1016/j.engfailanal.2022.106621.

[35] Kumagai N, Ishikawa H, Haga K, Kigawa T, Nagase K. Factors of wheel flats occurrence and preventive measures. Wear. 1991;144(1–2):277–87.

[36] Day AJ, Tirovic M, Newcomb TP. Thermal effects and pressure distributions in brakes. Proc Inst Mech Eng Part D J Automob Eng. 1991;205(3):199–206.

[37] Kalousek J, Magel E, Strasser J, Caldwell WN, Kanevsky G, Blevins B. Tribological interrelationship of seasonal fluctuations of freight car wheel wear, contact fatigue shelling and composition brakeshoe consumption. Wear. 1996;191(1–2):210–8.

[38] Martín Meizoso A, Martínez Esnaola JM, Fuentes Pérez M. Approximate crack growth estimate of railway wheel influenced by normal and shear action. Theor Appl Fract Mech. 1991;15(2):179–90.

[39] Zerbst U, Mädler K, Hintze H. Fracture mechanics in railway applications - An overview. Eng Fract Mech. 2008;72(2):163–94.
[40] Dufrénoy P, Bodovillé G, Degallaix G. Damage mechanisms and thermomechanical loading of brake discs. Eur Struct Integr Soc. 2002;29:167–76.
[41] Seo JW, Goo BC, Choi JB, Kim YJ. Effects of metal removal and residual stress on the contact fatigue life of railway wheels. Int J Fatigue. 2008;30(10–11):2021–9.
[42] Cristol-Bulthé AL, Desplanques Y, Degallaix G. Coupling between friction physical mechanisms and transient thermal phenomena involved in pad-disc contact during railway braking. Wear. 2007;263(7–12):1230–42.
[43] Ekberg A, Kabo E. Fatigue of railway wheels and rails under rolling contact and thermal loading-an overview. Wear. 2005;258(7–8):1288–300.
[44] Wang Z, Han J, Domblesky JP, Li Z, Fan X, Liu X. Crack propagation and microstructural transformation on the friction surface of a high-speed railway brake disc. Wear. 2019;428–429:45–54. doi: 10.1016/j.wear.2019.01.124.
[45] Wu X, Rakheja S, Cai W, Chi M, Ahmed AKW, Qu S. A study of formation of high order wheel polygonalization. Wear. 2019;424–425:1–14. doi: 10.1016/j.wear.2019.01.099.
[46] Makino T, Kato T, Hirakawa K. The effect of slip ratio on the rolling contact fatigue property of railway wheel steel. Int J Fatigue. 2012;36(1):68–79. doi: 10.1016/j.ijfatigue.2011.08.014.
[47] Masoudi Nejad R, Farhangdoost K, Shariati M. Numerical study on fatigue crack growth in railway wheels under the influence of residual stresses. Eng Fail Anal. 2015;52:75–89. doi: 10.1016/j.engfailanal.2015.03.002.
[48] Yang Y, Ling L, Wang C, Liu Z, Wang K, Zhai W. Wheel/rail dynamic interaction induced by polygonal wear of locomotive wheels. Veh Syst Dyn. 2022;60(1):211–35. doi: 10.1080/00423114.2020.1807572.
[49] Xie X, Li Z, Domblesky JP, Yang Z, Liu X, Li W, et al. Analysis of deep crack formation and propagation in railway brake discs. Eng Fail Anal. 2021;128:105600. doi: 10.1016/j.engfailanal.2021.105600.
[50] Lu C, Shen J, Fu Q, Mo J. Research on radial crack propagation of railway brake disc under emergency braking conditions. Eng Fail Anal. 2023;143:106877. doi: 10.1016/j.engfailanal.2022.106877.
[51] Masoudi Nejad R, Liu Z, Ma W, Berto F. Reliability analysis of fatigue crack growth for rail steel under variable amplitude service loading conditions and wear. Int J Fatigue. 2021;152:106450. doi: 10.1016/j.ijfatigue.2021.106450.
[52] East Japan Railway Company. Integrated report 2022. Vol. 991. 2022. https://www.jreast.co.jp/e/environment/pdf_2022/p048-061.pdf.
[53] Company EJR. CSR report 2016. 2016. https://www.jreast.co.jp/e/environment/2016.html.
[54] East Japan Railway Company. CSR report 2017 [Internet]. 2017. https://www.jreast.co.jp/e/environment/2017.html.
[55] Company EJR. Sustainability report 2019. Vol. 44. 2018. https://www.jreast.co.jp/e/environment/2018.html.
[56] East Japan Railway Company. Sustainability report 2019 [Internet]. 2019. https://www.jreast.co.jp/e/environment/2019.html.
[57] Company EJR. Integrated report 2020. 2020. https://www.jreast.co.jp/e/environment/2020.html.
[58] East Japan Railway Company. Integrated report 2021. 2021. https://www.jreast.co.jp/e/environment/pdf_2021/all.pdf.
[59] European Union Agency for Railways. European Union Agency for Railways - About us [Internet]. 2016. http://www.era.europa.eu/The-Agency/About-us/Pages/Home.aspx.
[60] Railways EUA for. European Railway Agency (ERA): Report on railway safety and interoperability in the EU 2018 [Internet]. 2018. https://www.era.europa.eu/sites/default/files/library/docs/safety_interoperability_progress_reports/railway_safety_and_interoperability_in_eu_2018_en.pdf.
[61] European Union Agency for Railways. Report on railway safety and interoperability in the EU. 2020. https://www.era.europa.eu/content/report-railway-safety-and-interoperability-eu-2020_en.
[62] European Union Agency for Railways. Report on railway safety and interoperability in the EU, 2022. 2022. https://www.era.europa.eu/content/report-railway-safety-and-interoperability-eu-2022_en.
[63] Charlton L. Rail safety statistics 2018-19 annual statistical release. 2019. https://dataportal.orr.gov.uk/media/1451/rail-safety-statistical-release-2018-19.pdf.
[64] Charlton L. Rail safety 2019-20. 2020. https://dataportal.orr.gov.uk/media/1832/rail-safety-2019-20.pdf.
[65] Ramyead A. Rail safety 2020-21. 2021. https://dataportal.orr.gov.uk/media/1999/rail-safety-2020-2021.pdf.
[66] Ramyead A. Rail safety April 2021 to March 2022. 2022. https://dataportal.orr.gov.uk/media/2131/rail-safety-april-2021-to-march-2022.pdf.
[67] Chen SZ, Lin JHC, Ju CP. Effect of aluminum content on tribological behavior of a Cu–Fe–C based friction material sliding against FC30 cast iron. Mater Trans. 2003;44(4):787–93.
[68] Chen SZ, Lin JHC, Ju CP. Effect of graphite content on the tribological behavior of a Cu–Fe–C based friction material sliding against FC30 cast iron. Mater Trans. 2003;44(6):1225–30.
[69] Ghaderi AR, Nili Ahmadabadi M, Ghasemi HM. Effect of graphite morphologies on the tribological behavior of austempered cast iron. Wear. 2003;255(1–6):410–6.
[70] Hirasata K, Hayashi K, Inamoto Y. Friction and wear of several kinds of cast irons under severe sliding conditions. Wear. 2007;263(1–6):790–800.
[71] Ertan R, Yavuz N. Optimisation of brake friction material on tribological characteristics and cost using constrained mixture design method. Int J Mater Prod Technol. 2010;39(3–4):271–90.
[72] Arjmand M, Shojaei A. Tribological characteristics of rubber-based friction materials. Tribol Lett. 2011;41(2):325–36.
[73] Shojaei A, Arjmand M, Saffar A. Studies on the friction and wear characteristics of rubber-based friction materials containing carbon and cellulose fibers. J Mater Sci. 2011;46(6):1890–901.
[74] Cui G, Bi Q, Zhu S, Fu L, Yang J, Qiao Z, et al. Synergistic effect of alumina and graphite on bronze matrix composites: tribological behaviors in sea water. Wear. 2013;303(1–2):216–24. doi: 10.1016/j.wear.2013.03.027.
[75] Surojo E, Jamasri, Malau V, Ilman MN. Effects of phenolic resin and fly ash on coefficient of friction of brake shoe composite. ARPN J Eng Appl Sci. 2014;9(11):2234–40.
[76] Surojo E, Jamasri, Malau V, Ilman MN. Investigation of friction behaviors of brake shoe materials using metallic filler. Tribol Ind. 2015;37(4):473–81.
[77] Li G, Yan Q. Comparison of friction and wear behavior between C/C, C/C-SiC and metallic composite materials. Tribol Lett. 2015;60(1):1–8.
[78] Ertan R. Synergistic effect of organic and ceramic based ingredients on the tribological characteristics of brake friction materials. Mater Tehnol. 2016;50(2):223–8.
[79] Maulana IT, Surojo E, Muhayat N, Raharjo WW. Frictional characteristics of friction brake material using cantala fibers as reinforcement. Tribol Online. 2018;13(4):188–94.

[80] Choosri S, Sombatsompop N, Wimolmala E, Thongsang S. Potential use of fly ash and bagasse ash as secondary abrasives in phenolic composites for eco-friendly brake pads applications. Proc Inst Mech Eng Part D J Automob Eng. 2018;233(5):1296–305.
[81] Ghosh P, Banerjee SS, Khastgir D. Elastomer modified phenolic resin-based composites with reduced scale friction: influence of calcined petroleum coke on tribological and thermo-mechanical behavior. Polym Eng Sci. 2020;60(7):1446–58.
[82] Palmiyanto MH, Surojo E, Ariawan D, Imaduddin F. Waste glass powder as a sustainable abrasive material for composite brake block. Tribol Ind. 2021;43(3):363–72.
[83] Monreal P, Oroz J, Gutiérrez K, Clavería Ambroj I. Natural latxa sheep wool as an environmentally friendly substitute for specific organic fibers in railway friction materials: a preliminary approach. Tribol Trans. 2021;64(5):851–63. doi: 10.1080/10402004.2021.1939210.
[84] Yanar H, Purcek G, Demirtas M, Huseyin H. Effect of hexagonal boron nitride (h-BN) addition on friction behavior of low-steel composite brake pad material for railway applications. Tribol Int. 2022;165:107274. doi: 10.1016/j.triboint.2021.107274.
[85] Sunardi S, Ariawan D, Surojo E, Prabowo AR, Akbar HI, Sudrajad A, et al. Optimization of eggshell particles to produce ecofriendly green fillers with bamboo reinforcement in organic friction materials. Rev Adv Mater Sci. 2023;62(1):20230111.
[86] Ajayi JA, Adeleke OA. Failure analysis of railway brake blocks. Eng Fail Anal. 1997;4(3):205–13.
[87] Laden K, Guérin JD, Watremez M, Bricout JP. Frictional characteristics of Al–SiC composite brake discs. Tribol Lett. 2000;8(4):237–47.
[88] Abbasi F, Shojaei A, Katbab AA. Thermal interaction between polymer-based composite friction materials and counterfaces. J Appl Polym Sci. 2001;81(2):364–9.
[89] Wang H, Wu X, Liu X, Cong P. Application study of a modified phenolic resin as binder for hybrid fibers reinforced brake pad for railroad passenger-coach braking. J Macromol Sci Part A Pure Appl Chem. 2011;48(4):261–70.
[90] Wang H, Zhuang G, Wang C, Zheng S. Practical application study of hybrid fibers reinforced organic brake pad for railroad passenger-coach braking. J Macromol Sci Part A Pure Appl Chem. 2011;48(7):531–7.
[91] Baklouti M, Elleuch R, Cristol AL, Najjar D, Desplanques Y. Relationships between the heterogeneous microstructure, the mechanical properties and the braking behaviour of an organic brake lining material. Proc Inst Mech Eng Part D J Automob Eng. 2013;227(4):549–60.
[92] Surojo E, Jamasri, Malau V, Ilman MN. Characteristic evaluation of brake block material. Tribol Ind. 2017;39(4):527–35.
[93] Peng T, Yan Q, Li G, Zhang X. The influence of Cu/Fe ratio on the tribological behavior of brake friction materials. Tribol Lett. 2018;66(1):1–12. doi: 10.1007/s11249-017-0961-2.
[94] Sugözü B. Tribological properties of brake friction materials containing fly ash. Ind Lubr Tribol. 2018;70(5):902–6.
[95] Zhang P, Zhang L, Fu K, Wu P, Cao J, Shijia C, et al. Effects of Ni-coated graphite flake on braking behavior of Cu-based brake pads applied in high-speed railway trains. J Tribol. 2019;141(8):1–14.
[96] Zhang P, Zhang L, Wei D, Wu P, Cao J, Shijia C, et al. A high-performance copper-based brake pad for high-speed railway trains and its surface substance evolution and wear mechanism at high temperature. Wear. 2020;444–445:203182. doi: 10.1016/j.wear.2019.203182.
[97] Wang J, Zafar MQ, Chen Y, Pan P, Zuo L, Zhao H, et al. Tribological properties of brake disc material for a high-speed train and the evolution of debris. Lubricants. 2022;10(8):168.